

Supporting Information for

Four-Electron Oxidation and One-Electron Reduction of the Bis(terphenylthiolate) U(II) Complex, U(SAr^{iPr6})₂ [Ar^{iPr6} = C₆H₃-2,6-(C₆H₂-2,4,6-ⁱPr₃)₂]

Joshua D. Queen, Eric Ma, Ahmadreza Rajabi, Joseph W. Ziller, Filipp Furche* and William J. Evans*

Department of Chemistry, University of California, Irvine, California, 92697, United States

Table of Contents

Experimental Details	S2
Discussion of 1	S5
X-ray crystallography	S6
Cyclic Voltammetry	S13
NMR Spectra	S14
UV-Visible Spectra	S19
Infrared Spectra	S23
Computational Details	S27
Ground-State Geometries and Energetics	S27
Optimized Geometries for Different Spin States and Relative Energies	S27
Population Analyses of Kohn-Sham Molecular Orbitals	S30
Simulation and Characterization of Electronic Spectra from TDDFT	S36
Discussion	S38
References	S39

Experimental Details

General Procedures. All manipulations were performed by using modified Schlenk techniques or in a Vacuum Atmospheres glovebox under nitrogen or argon. Solvents were degassed by sparging with dry argon before drying and collection using an S2 Grubbs-type solvent purification system (JC Meyer). All physical measurements were recorded under strictly anaerobic and anhydrous conditions. Infrared spectra were recorded on compressed solid samples using an Agilent Cary 630 ATR/FTIR instrument. UV-visible spectra were recorded as dilute solutions in the indicated solvent in quartz cuvettes (1 mm path length) using an Agilent Cary 60 UV/vis spectrophotometer. Combustion analyses were performed using a Thermo Scientific FlashSmart CHNS/O Elemental Analyzer. NMR spectra were recorded using Bruker AVANCE 600 MHz NMR spectrometer and referenced to residual solvent signals for ^1H and $^{13}\text{C}\{^1\text{H}\}$.¹ Solution magnetic moments were measured using Evans' method and estimated diamagnetic corrections.²⁻⁴ Electrochemical measurements were collected under argon with a freshly made THF solution of $[\text{nBu}_4\text{N}][\text{BPh}_4]$ with a glassy carbon working electrode, platinum wire counter electrode, and silver wire pseudo-reference electrode using a Princeton Applied Research PARSTAT 2273 Advanced Electrochemical System and were referenced with an internal standard of $(\text{C}_5\text{Me}_5)_2\text{Fe}$. Internal resistance was measured and resistance was manually compensated by approximately 90% of the measured value. $[\text{K}(\mu\text{-SAr}^{\text{iPr}_6})_2]$,⁵ UI_3 ,⁶ and KC_8 ⁷ prepared according to the literature procedures. Azobenzene was obtained commercially and used without further purification.

Caution! ^{238}U is radioactive and an α emitter with a half-life of approximately 4.5×10^9 years. Studies were conducted in a laboratory with appropriate radiological safety equipment.

$\text{U}(\text{SAr}^{\text{iPr}_6})_2\mathbf{1}$. Inside the glovebox, solid $[\text{K}(\mu\text{-SAr}^{\text{iPr}_6})_2]$ (0.300 g, 0.271 mmol) and UI_3 (0.168 g, 0.271 mmol) were combined in a 20 mL scintillation vial and Et_2O (*ca.* 15 mL) was added. The resulting purple mixture was stirred overnight. Then the solvent was removed under vacuum and the residue extracted with two *ca.* 10 mL portions of *n*-hexane. The extracts were centrifuged and filtered through a pipette packed with Kimwipes. The dark purple supernatant solution was slowly concentrated to *ca.* 8 mL under reduced pressure and stored at -35°C to afford dark purple block shaped crystals of $\mathbf{1} \cdot 1.5\text{C}_6\text{H}_{14}$ (0.281 g, 0.202 mmol, 74%). Anal. Calcd for $\text{C}_{72}\text{H}_{98}\text{S}_2\text{UI}$: C, 62.10; H, 7.09; S, 4.61. Found: C, 62.66; H, 7.46; S, 4.93. ^1H NMR (500 MHz, C_6D_6 , 298 K): δ ($\Delta\nu_{1/2}$),

22.4 (230 Hz), 15.5 (230 Hz), 14.4 (200 Hz), 13.7 (250 Hz), 10.4 (200 Hz), 9.7 (250 Hz), 8.1 (14 Hz), 7.9 (240 Hz), 4.8 (220 Hz), 3.6 (140 Hz), 3.0 (200 Hz), 2.5 (200 Hz), -1.4 (220 Hz), -3.0 (250 Hz), -7.9 (230 Hz), -11.9 (270 Hz), -22.1 (330 Hz), -35.9 (300 Hz). Magnetic moment (Evans, benzene): 2.7 μ_B . UV-vis (*n*-hexane); λ_{max} , nm (ϵ , L mol⁻¹ cm⁻¹): 475 (1500), 484 (shoulder, 1400), 565 (shoulder, 1100), 613 (shoulder, 800), 655 (shoulder, 500). ATR-FTIR (cm⁻¹): 2956s, 2927m, 2866m, 1060w, 1587w, 1569w, 1537w, 1458s, 1413m, 1386s, 1361m, 1334w, 1316m, 1248w, 1189w, 1168w, 1150w, 1108m, 1082w, 1069w, 1044m, 1004w, 938w, 897m, 874m, 848w, 793m, 770w, 743s, 730s.

U(SAr^{iPr})₂, 2. Inside the glovebox, KC₈ (0.022 g, 0.16 mmol) was added in one portion to a stirred purple solution of **1** (0.210 g, 0.151 mmol) in *ca.* 15 mL of Et₂O at ambient temperature and the mixture was stirred overnight. The mixture was centrifuged and the dark green supernatant solution was filtered through a pipette packed with Kimwipes. The solvent was removed under vacuum to afford a sticky dark green residue that was triturated twice with 1 mL portions of SiMe₄ to afford **2** as a dark green powder (0.160 g, 0.126 mmol, 84%). Anal. Calcd for C₇₂H₉₈S₂U: C, 68.32; H, 7.80; S, 5.07. Found: C, 68.56; H, 8.04; S: 5.33. Slow evaporation of a solution of *ca.* 20 mg of **2** in *ca.* 2 mL of *n*-hexane inside the glovebox afforded several green-brown needles that were suitable for X-ray diffraction. ¹H NMR (500 MHz, C₆D₆, 298 K): 15.1 ($\Delta\nu_{1/2}$ = 169 Hz), 12.0 (s), 7.52 (d, *J* = 7.1 Hz), 4.62 (d, *J* = 7.7 Hz), 4.15 (t, *J* = 7.4 Hz), 3.52 ($\Delta\nu_{1/2}$ = 137 Hz), 1.38 (mult), 0.92, 0.29, -0.17, -2.7 ($\Delta\nu_{1/2}$ = 129 Hz), -3.8 ($\Delta\nu_{1/2}$ = 147 Hz), -5.9 ($\Delta\nu_{1/2}$ = 157 Hz), -27.8 ($\Delta\nu_{1/2}$ = 198 Hz). Magnetic moment (Evans, benzene): 2.8 μ_B . UV-vis (*n*-hexane); λ_{max} , nm (ϵ , L mol⁻¹ cm⁻¹): 410 (shoulder, 3000). ATR-FTIR (cm⁻¹): 2954s, 2925m, 2863m, 1604w, 1567w, 1457m, 1382s, 1359m, 1315w, 1246m, 1167w, 1104w, 1069w, 1044m, 938w, 923w, 858s, 792m, 744s, 730s, 693m.

U(SAr^{iPr})₂(=NPh)₂(THF)₂, 3. To a solution of **2** (0.100 g, 0.079 mmol) in hexane (*ca.* 5 mL), azobenzene (0.015 g 0.082 mmol) was added in one portion. The mixture was stirred 10 min during which time the color changed from dark green to dark red-brown. The supernatant solution was separated by centrifuge and filtered through a pipette packed with Kimwipes. A small amount of THF (*ca.* 0.3 mL) was added and the solution was concentrated to *ca.* 0.5 mL under vacuum and stored at -35°C for one day to afford brown crystals of **3** (0.073 g, 0.049 mmol, 62%). Anal.

Calcd for $C_{92}H_{124}O_2N_2S_2U$: C, 69.40; H, 7.85; N, 1.76; S, 4.03. Found: C, 69.49; H, 8.04; N, 1.70; S, 3.80. UV-vis (*n*-hexane); λ_{max} , nm (ϵ , $L\ mol^{-1}\ cm^{-1}$): 465 (2600). ATR-FTIR (cm^{-1}): 2956s, 2926m, 2863m, 1602w, 1565w, 1458s, 1379s, 1359m, 1314w, 1297w, 1257s, 1165w, 1100w, 1067w, 1063m, 1000w, 997w, 950m, 921w, 874m, 818w, 799m, 775m, 750s, 730s, 690s.

UK(μ -SAr^{*i*Pr⁶})₂, 4. Inside the glovebox, solid KC_8 (7 mg, 0.052 mmol) was added to a solution of **2** (65 mg, 0.051 mmol) in Et_2O (*ca.* 4 mL) and the mixture stirred for 5 min, resulting in a color change from dark green to dark brown. The supernatant solution was filtered through a pipette packed with Kimwipes and concentrated to *ca.* 0.5 mL under vacuum. To this *ca.* 0.5 mL of *n*-hexane was added and the mixture was stored at $-35^\circ C$ for two days to afford dark brown block shaped crystals of **3** suitable for X-ray crystallography (0.059 g, 0.045 mmol, 88%). Anal. Calcd for $C_{72}H_{98}S_2UK$: C, 66.28; H, 7.57; S, 4.91. Found: C, 66.72; H, 7.91; S, 4.80. Magnetic moment (Evans, benzene): 2.4 μB . UV-vis (Et_2O); λ_{max} , nm (ϵ , $L\ mol^{-1}\ cm^{-1}$): 275 (50000), 400 (shoulder, 8000). ATR-FTIR (cm^{-1}): 2953s, 2924m, 2862m, 1603w, 1565w, 1457s, 1381s, 1358m, 1315w, 1286w, 1254w, 1238w, 1166w, 1103w, 1079w, 1069w, 1044m, 938w, 920w, 874m, 845w, 790w, 783m, 742s, 230s, 694w.

Discussion of $U(\text{SAr}^{\text{iPr6}})_2\text{I}$, **1**.

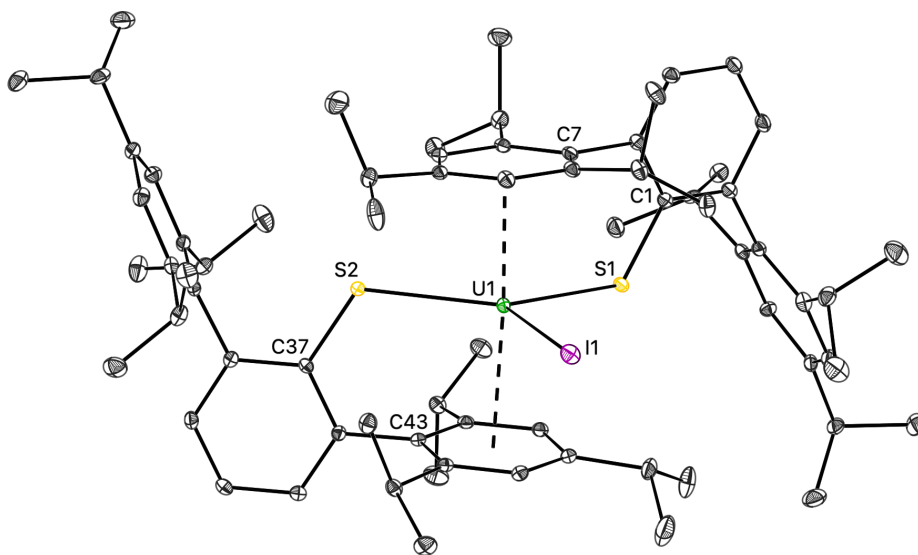


Figure S1. Molecular structure of $U(\text{SAr}^{\text{iPr6}})_2\text{I}$, **1**, with ellipsoids drawn at 30% probability. Hydrogen atoms, disordered carbon atoms of the terphenyl rings, and n-hexane solvent molecules not shown for clarity.

The 2.7590(5) and 2.8226(5) Å U–S bonds in **1** are similar to the 2.7888(8) and 2.7969(7) Å lengths in $U(\text{SAr}^{\text{iPr6}})_2(\text{BH}_4)$, all of which are longer than the average 2.720(5) Å U–S distance in $U(\text{SC}_6\text{H}_2^t\text{Bu}_3)_3$ ⁸ and the 2.7082(7) Å U–S bonds in $[\text{mes}^{\text{(Me,Ad)ArS}}]_3\text{U}^{\text{III}}$.⁹ The 2.724(1) and 2.800(1) Å U–Cnt distances (Cnt = the centroid of a flanking C_6 ring) are comparable to those in $U(\text{NHAr}^{\text{iPr6}})_2\text{I}$ (2.777(1), 2.790(1) Å) and in $U(\text{SAr}^{\text{iPr6}})_2(\text{BH}_4)$ (2.744(2), 2.747(2) Å). The $173.68(3)^\circ$ Cnt–U–Cnt angle is wider than that in $U(\text{NHAr}^{\text{iPr6}})_2\text{I}$ (158.79°) and close to those in $U(\text{SAr}^{\text{iPr6}})_2(\text{BH}_4)$ (176.80°) and $\text{Ln}(\text{SAr}^{\text{iPr6}})_2\text{I}$ (Ln = La, $173.22(5)^\circ$; Nd, $175.38(1)^\circ$).

The 298 K solution magnetic moment of **1** was found to be 2.6–2.7 μ_{B} which is comparable to the related U(III) thiolates $U(\text{SAr}^{\text{iPr6}})(\text{BH}_4)_2$ ($\mu_{\text{eff}} = 2.47 \mu_{\text{B}}$) and $U(\text{SAr}^{\text{iPr6}})_2(\text{BH}_4)$ ($\mu_{\text{eff}} = 2.47 \mu_{\text{B}}$)¹⁰ Magnetic moments of U(III) compounds typically span a range of *ca.* 2.4–3.8 μ_{B} .¹¹

X-ray Crystallography

X-ray Data Collection, Structure Solution and Refinement for 1.

A purple crystal of approximate dimensions 0.070 x 0.135 x 0.309 mm was mounted in a cryoloop and transferred to a Bruker SMART APEX II diffractometer system. The APEX2^{12a} program package was used to determine the unit-cell parameters and for data collection (60 sec/frame scan time). The raw frame data was processed using SAINT^{13a} and SADABS^{14a} to yield the reflection data file. Subsequent calculations were carried out using the SHELXTL¹⁵ program package. There were no systematic absences nor any diffraction symmetry other than the Friedel condition. The centrosymmetric triclinic space group $P\bar{1}$ was assigned and later determined to be correct.

The structure was solved by direct methods and refined on F^2 by full-matrix least-squares techniques. The analytical scattering factors¹⁶ for neutral atoms were used throughout the analysis. Hydrogen atoms were included using a riding model.

Disorder related to libration of one of the ligand flanking rings was modeled as 0.67 and 0.33 occupancy of the two sites and thermal parameters of disordered atoms were restrained using SIMU DFIX and ISOR restraints/constraints.

One and one half hexane solvent molecules were contained in the asymmetric unit.

Least-squares analysis yielded $wR2 = 0.660$ and $Goof = 1.030$ for 935 variables refined against 22976 data (0.70 Å), $R1 = 0.0285$ for those 20167 data with $I > 2.0\sigma(I)$.

X-ray Data Collection, Structure Solution and Refinement for 2.

A brown crystal of approximate dimensions 0.331 x 0.066 x 0.043 mm was mounted in a cryoloop and transferred to a Bruker SMART APEX II diffractometer system. The APEX2^{12a} program package and the CELL_NOW¹⁷ were used to determine the unit-cell parameters. Data was collected using a 60 sec/frame scan time for a sphere of diffraction data. The raw frame data was processed using SAINT^{13a} and TWINABS¹⁸ to yield the reflection data file (HKL5 format)¹⁸. Subsequent calculations were carried out using the SHELXTL⁵ program package. There were no

systematic absences nor any diffraction symmetry other than the Friedel condition. The centrosymmetric triclinic space group $P\bar{1}$ was assigned and later determined to be correct.

The structure was solved by direct methods and refined on F^2 by full-matrix least-squares techniques. The analytical scattering factors¹⁶ for neutral atoms were used throughout the analysis. Hydrogen atoms were included using a riding model.

Restraints and constraints were applied to several carbon atoms in the ligands to achieve reasonable C-C distances and thermal parameters in the model.

Least-squares analysis yielded $wR2 = 0.2594$ and $Goof = 1.095$ for 692 variables refined against 13893 data (0.80 Å), $R1 = 0.1066$ for those 10620 with $I > 2.0\sigma(I)$. The structure was refined as a two-component twin, $BASF^5 = 0.331$.

There were several high residuals present in the final difference-Fourier map. It was not possible to determine the nature of the residuals although it was probable that *n*-hexane solvent was present. The SQUEEZE¹⁹ routine in the PLATON²⁰ program package was used to account for the electrons in the solvent accessible voids.

X-ray Data Collection, Structure Solution and Refinement for 3.

A brown crystal of approximate dimensions 0.278 x 0.274 x 0.096 mm was mounted in a cryoloop and transferred to a Bruker SMART APEX II diffractometer system. The APEX2^{12a} program package was used to determine the unit-cell parameters and for data collection (25 sec/frame scan time). The raw frame data was processed using SAINT^{13a} and SADABS^{14a} to yield the reflection data file. Subsequent calculations were carried out using the SHELXTL¹⁵ program package. The diffraction symmetry was $2/m$ and the systematic absences were consistent with the monoclinic space groups Cc , and $C2/c$. It was later determined that space group $C2c$ was correct.

The structure was solved by direct methods and refined on F^2 by full-matrix least-squares techniques. The analytical scattering factors¹⁶ for neutral atoms were used throughout the analysis. Hydrogen atoms were included using a riding model.

Least-squares analysis yielded $wR2 = 0.0789$ and $Goof = 1.029$ for 481 variables refined against 13043 data (0.73 Å), $R1 = 0.0288$ for those 9935 data with $I > 2.0\sigma(I)$.

There were several high residuals present in the final difference-Fourier map. It was not possible to determine the nature of the residuals although it was probable that *n*-hexane solvent was present. The SQUEEZE¹⁹ routine in the PLATON²⁰ program package was used to account for the electrons in the solvent accessible voids.

X-ray Data Collection, Structure Solution and Refinement for 4.

A black crystal of approximate dimensions 0.030 x 0.088 x 0.104 mm was mounted in a cryoloop and transferred to a Bruker D8 Advance Photon III diffractometer system. The APEX5^{12b} program package was used to determine the unit-cell parameters and for data collection (1 sec/frame scan time). The raw frame data was processed using SAINT^{13b} and SADABS^{14b} to yield the reflection data file. Subsequent calculations were carried out using the SHELXTL¹⁵ program package. The diffraction symmetry was $2/m$ and the systematic absences were consistent with the monoclinic space group $P21/n$ that was later determined to be correct.

The structure was solved by direct methods and refined on F2 by full-matrix least-squares techniques. The analytical scattering factors¹⁶ for neutral atoms were used throughout the analysis. Hydrogen atoms were included using a riding model.

There were several high residuals present in the final difference-Fourier map. It was not possible to determine the nature of the residuals although it was probable that *n*-hexane or diethyl ether solvent was present. The SQUEEZE routine¹⁹ in the PLATON program²⁰ package was used to account for the electrons in the solvent accessible voids.

Least-squares analysis yielded $wR2 = 0.1497$ and $Goof = 1.031$ for 718 variables refined against 11599 data (0.85 Å), $R1 = 0.0581$ for those 9328 data with $I > 2.0\sigma(I)$.

Table S1. Crystal data and structure refinement for **1**.

Identification code	jdq22	
Empirical formula	C ₈₁ H ₁₁₉ S ₂ IU	
Formula weight	1521.80	
Temperature	93(2) K	
Wavelength	0.71073 Å	
Crystal system	Triclinic	
Space group	<i>P</i> -1	
Unit cell dimensions	a = 13.4289(10) Å	α = 85.4100(10)°
	b = 14.0220(10) Å	β = 73.3550(10)°
	c = 21.4050(16) Å	γ = 80.4720(10)°
Volume	3806.1(5) Å ³	
Z	2	
Density (calculated)	1.328 Mg/m ³	
Absorption coefficient	2.633 mm ⁻¹	
F(000)	1564	
Crystal size	0.310 × 0.134 × 0.070 mm ³	
Theta range for data collection	2.007 to 30.556°.	
Index ranges	-18 ≤ h ≤ 18, -20 ≤ k ≤ 20, -30 ≤ l ≤ 30	
Reflections collected	99232	
Independent reflections	22976 [R(int) = 0.0399]	
Completeness to theta = 25.242°	99.9 %	
Absorption correction	Semi-empirical from equivalents	
Max. and min. transmission	0.746 and 0.572	
Refinement method	Full-matrix least-squares on F ²	
Data / restraints / parameters	22976 / 113 / 935	
Goodness-of-fit on F ²	1.030	
Final R indices [I > 2σ(I)]	R1 = 0.0285, wR2 = 0.0634	
R indices (all data)	R1 = 0.0368, wR2 = 0.0660	
Largest diff. peak and hole	2.155 and -0.956 e.Å ⁻³	

Table S2. Crystal data and structure refinement for **2**.

Identification code	jdq35	
Empirical formula	C ₇₂ H ₉₈ S ₂ U	
Formula weight	1265.65	
Temperature	93(2) K	
Wavelength	0.71073 Å	
Crystal system	Triclinic	
Space group	<i>P</i> -1	
Unit cell dimensions	a = 9.864(9) Å	α = 87.762(11)°
	b = 17.520(16) Å	β = 84.587(10)°
	c = 20.169(18) Å	γ = 85.962(10)°
Volume	3460(5) Å ³	
Z	2	
Density (calculated)	1.215 Mg/m ³	
Absorption coefficient	2.443 mm ⁻¹	
F(000)	1308	
Crystal size	0.331 × 0.066 × 0.043 mm ³	
Theta range for data collection	2.078 to 26.284°.	
Index ranges	-12 ≤ h ≤ 12, -21 ≤ k ≤ 21, 0 ≤ l ≤ 25	
Reflections collected	13893	
Independent reflections	13893 [R(int) = 0.1240]	
Completeness to theta = 25.242°	100.0 %	
Absorption correction	Semi-empirical from equivalents	
Max. and min. transmission	0.745 and 0.447	
Refinement method	Full-matrix least-squares on F ²	
Data / restraints / parameters	13893 / 283 / 692	
Goodness-of-fit on F ²	1.095	
Final R indices [I > 2σ(I)]	R1 = 0.1066, wR2 = 0.2594	
R indices (all data)	R1 = 0.1312, wR2 = 0.2753	
Extinction coefficient	0.040(2)	
Largest diff. peak and hole	6.087 and -4.216 e.Å ⁻³	

Table S3. Crystal data and structure refinement for **3**.

Identification code	jdq23	
Empirical formula	C ₉₂ H ₁₂₄ N ₂ O ₂ S ₂ U	
Formula weight	1592.07	
Temperature	133(2) K	
Wavelength	0.71073 Å	
Crystal system	Monoclinic	
Space group	C2/c	
Unit cell dimensions	a = 30.491(5) Å	α = 90°
	b = 18.735(3) Å	β = 113.138(2)°
	c = 18.433(3) Å	γ = 90°
Volume	9683(3) Å ³	
Z	4	
Density (calculated)	1.092 Mg/m ³	
Absorption coefficient	1.760 mm ⁻¹	
F(000)	3320	
Crystal size	0.278 × 0.274 × 0.096 mm ³	
Theta range for data collection	1.307 to 29.130°.	
Index ranges	-41 ≤ h ≤ 41, -25 ≤ k ≤ 25, -25 ≤ l ≤ 25	
Reflections collected	71568	
Independent reflections	13043 [R(int) = 0.0408]	
Completeness to theta = 25.242°	100.0 %	
Absorption correction	Semi-empirical from equivalents	
Max. and min. transmission	0.746 and 0.661	
Refinement method	Full-matrix least-squares on F ²	
Data / restraints / parameters	13043 / 52 / 481	
Goodness-of-fit on F ²	1.029	
Final R indices [I > 2σ(I)]	R1 = 0.0288, wR2 = 0.0725	
R indices (all data)	R1 = 0.0429, wR2 = 0.0789	
Largest diff. peak and hole	1.739 and -1.051 e.Å ⁻³	

Table S4. Crystal data and structure refinement for **4**.

Identification code	jdq38	
Empirical formula	C ₇₂ H ₉₈ S ₂ KU	
Formula weight	1304.75	
Temperature	110(2) K	
Wavelength	1.54178 Å	
Crystal system	Monoclinic	
Space group	<i>P</i> 2 ₁ / <i>n</i>	
Unit cell dimensions	a = 14.2720(3) Å	α = 90°
	b = 19.9414(4) Å	β = 98.185(2)°
	c = 24.2485(5) Å	γ = 90°
Volume	6830.9(2) Å ³	
Z	4	
Density (calculated)	1.269 Mg/m ³	
Absorption coefficient	8.074 mm ⁻¹	
F(000)	2692	
Crystal size	0.104 × 0.088 × 0.030 mm ³	
Theta range for data collection	2.881 to 65.308°	
Index ranges	-16 ≤ h ≤ 6, -23 ≤ k ≤ 20, -28 ≤ l ≤ 28	
Reflections collected	103487	
Independent reflections	11599 [R(int) = 0.1284]	
Completeness to theta = 65.308°	99.1 %	
Absorption correction	Semi-empirical from equivalents	
Refinement method	Full-matrix least-squares on F ²	
Data / restraints / parameters	11599 / 6 / 718	
Goodness-of-fit on F ²	1.031	
Final R indices [I > 2σ(I)]	R1 = 0.0581, wR2 = 0.1399	
R indices (all data)	R1 = 0.0752, wR2 = 0.1497	
Largest diff. peak and hole	2.365 and -1.931 e.Å ⁻³	

Cyclic Voltammetry

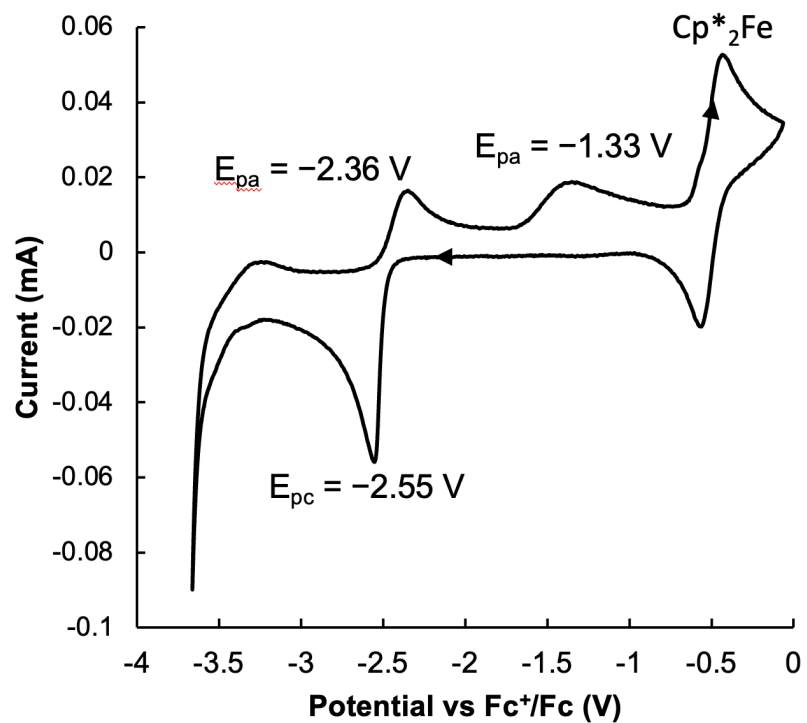


Figure S2. Cyclic voltammogram of U(SAr^{iPr}₆)₂, **2** in a *ca.* 100 mM [ⁿBu₄N][BPh₄] solution in THF. A scan rate of 200 mV sec⁻¹ was used.

NMR Spectra

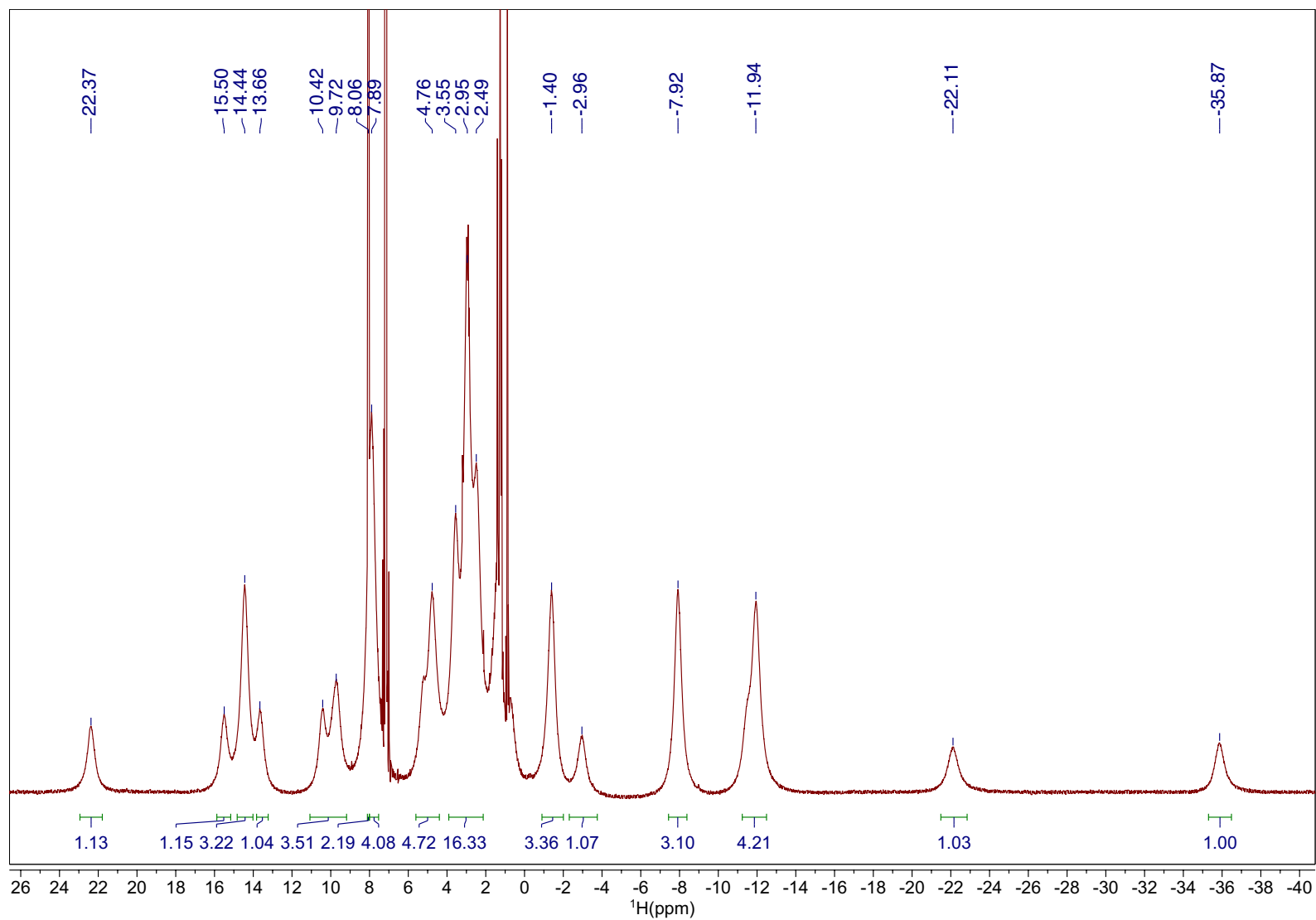


Figure S3. The paramagnetic ^1H NMR (500 MHz, 298 K) of $\text{UI}(\text{SAr}^{\text{iPr}_6})_2$, **1**, in C_6D_6 .

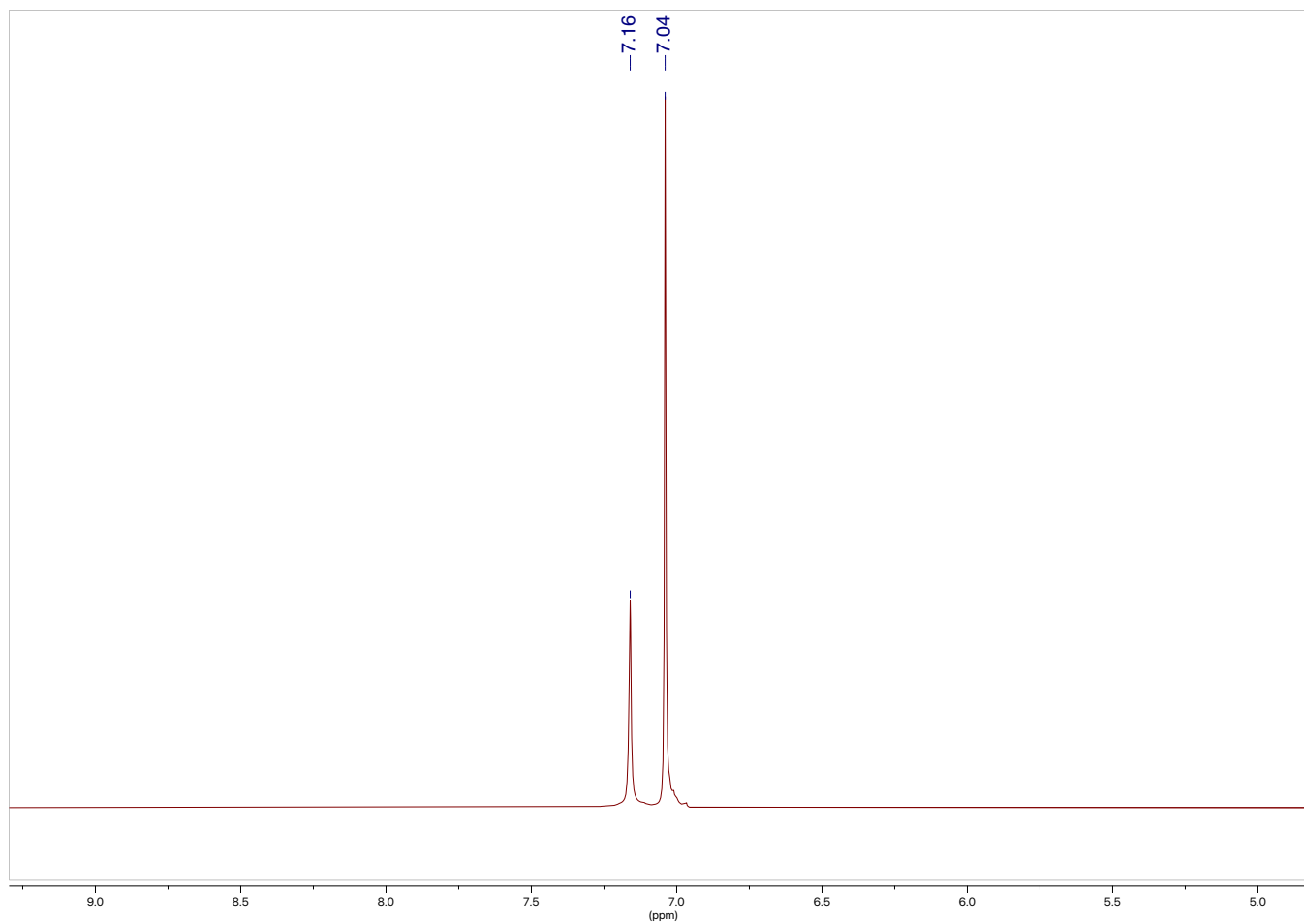


Figure S4. The ¹H NMR (500 MHz, 298 K) used for Evans' method magnetic moment determination of UI(SAr^{iPr6})₂, **1**, in C₆D₆. The concentration is 13 mM and an estimated diamagnetic correction of $-880 \times 10^{-6} \text{ emu mol}^{-1}$ was used.

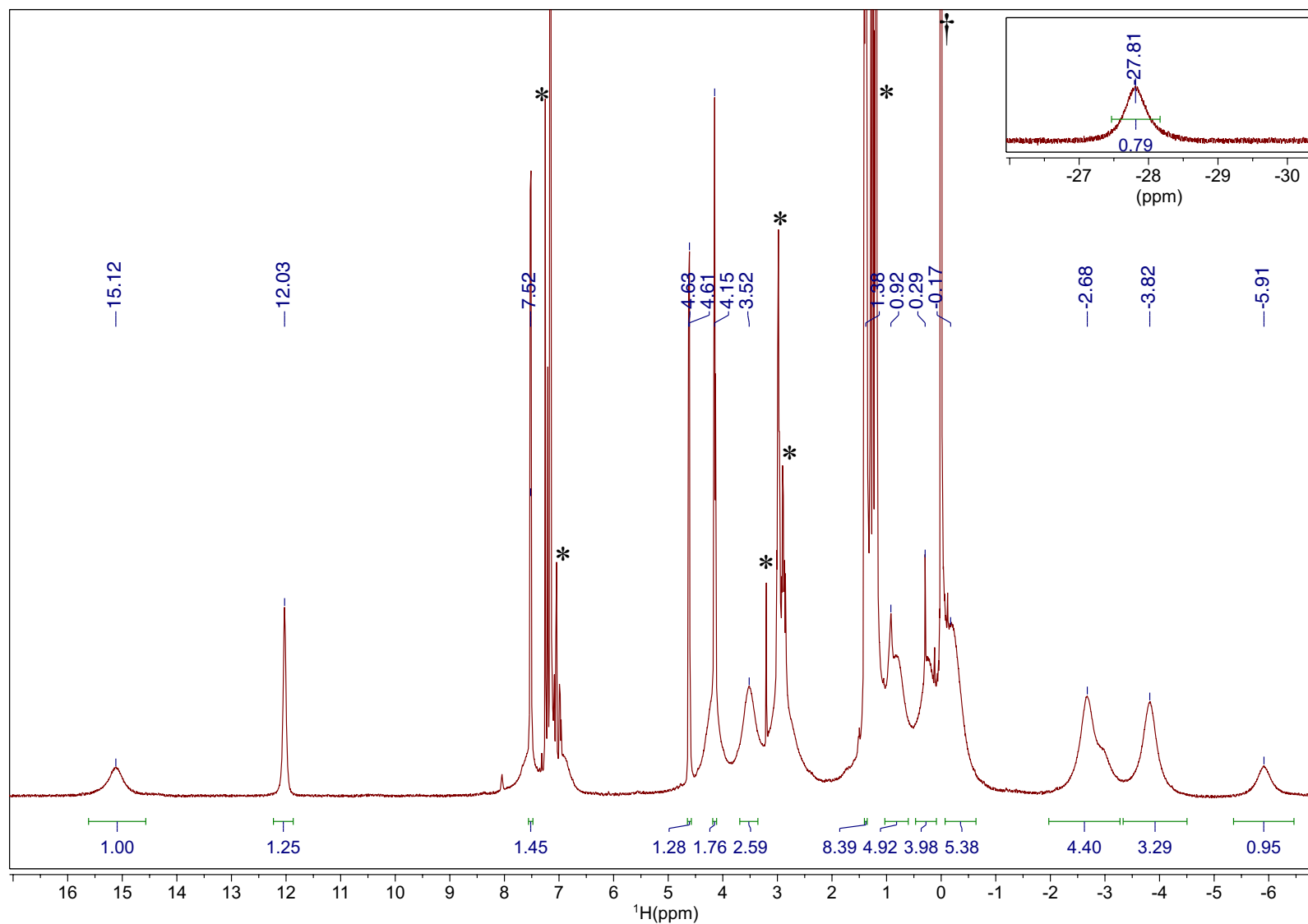


Figure S5. The paramagnetic ^1H NMR (500 MHz, 298 K) of $\text{U}(\text{SAr}^{\text{iPr}_6})_2$, **2**, in C_6D_6 . An impurity of $\text{HSAr}^{\text{iPr}_6}$ (*) is present due to the high sensitivity of **2** towards trace moisture. The peak at 0.00 ppm (†) is residual SiMe_4 .

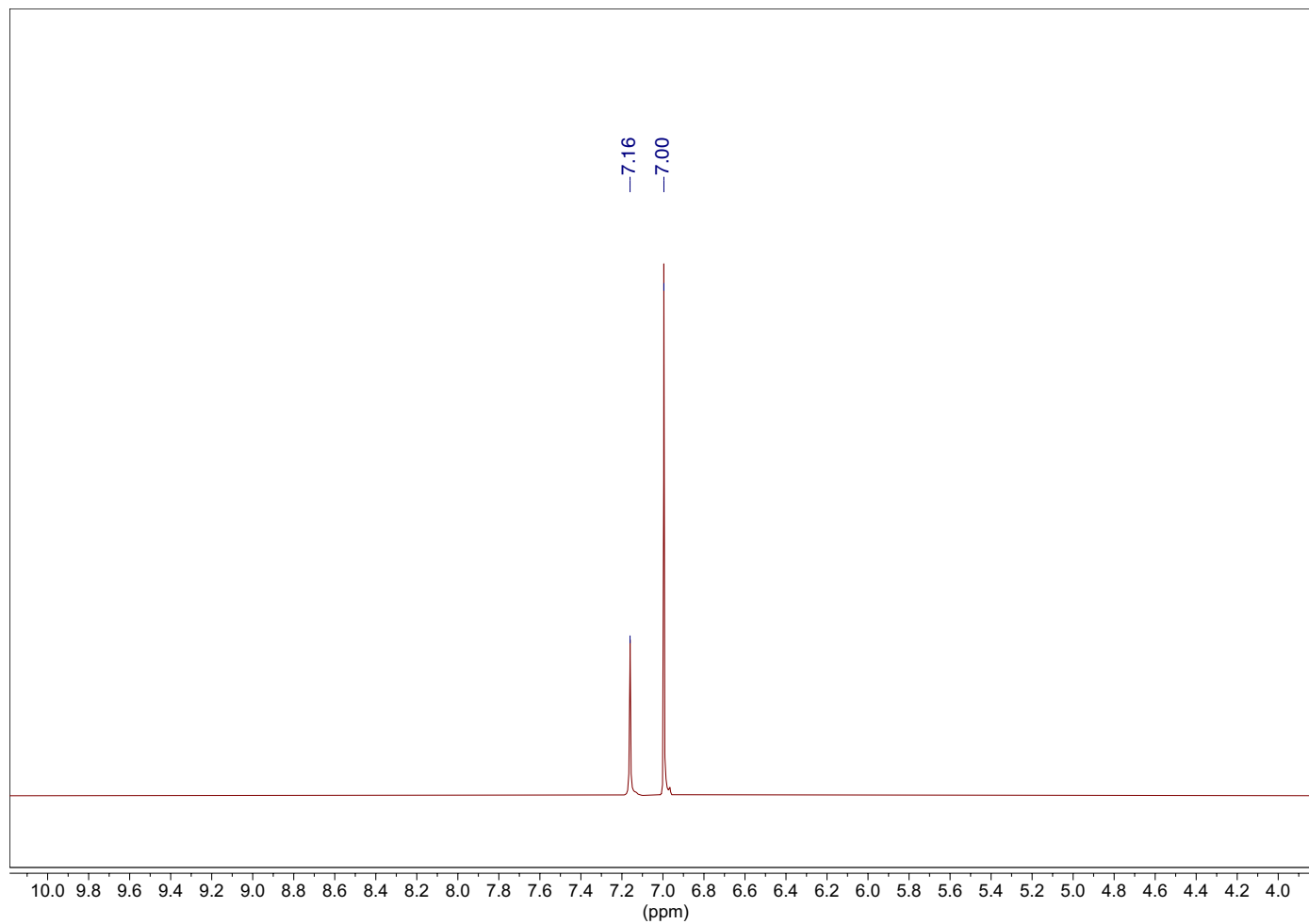


Figure S6. The ¹H NMR (500 MHz, 298 K) used for Evans' method magnetic moment determination of U(SAr^{iPr6})₂, **2**, in C₆D₆. The concentration is 16 mM and an estimated diamagnetic correction of $-835 \times 10^{-6} \text{ emu mol}^{-1}$ was used.

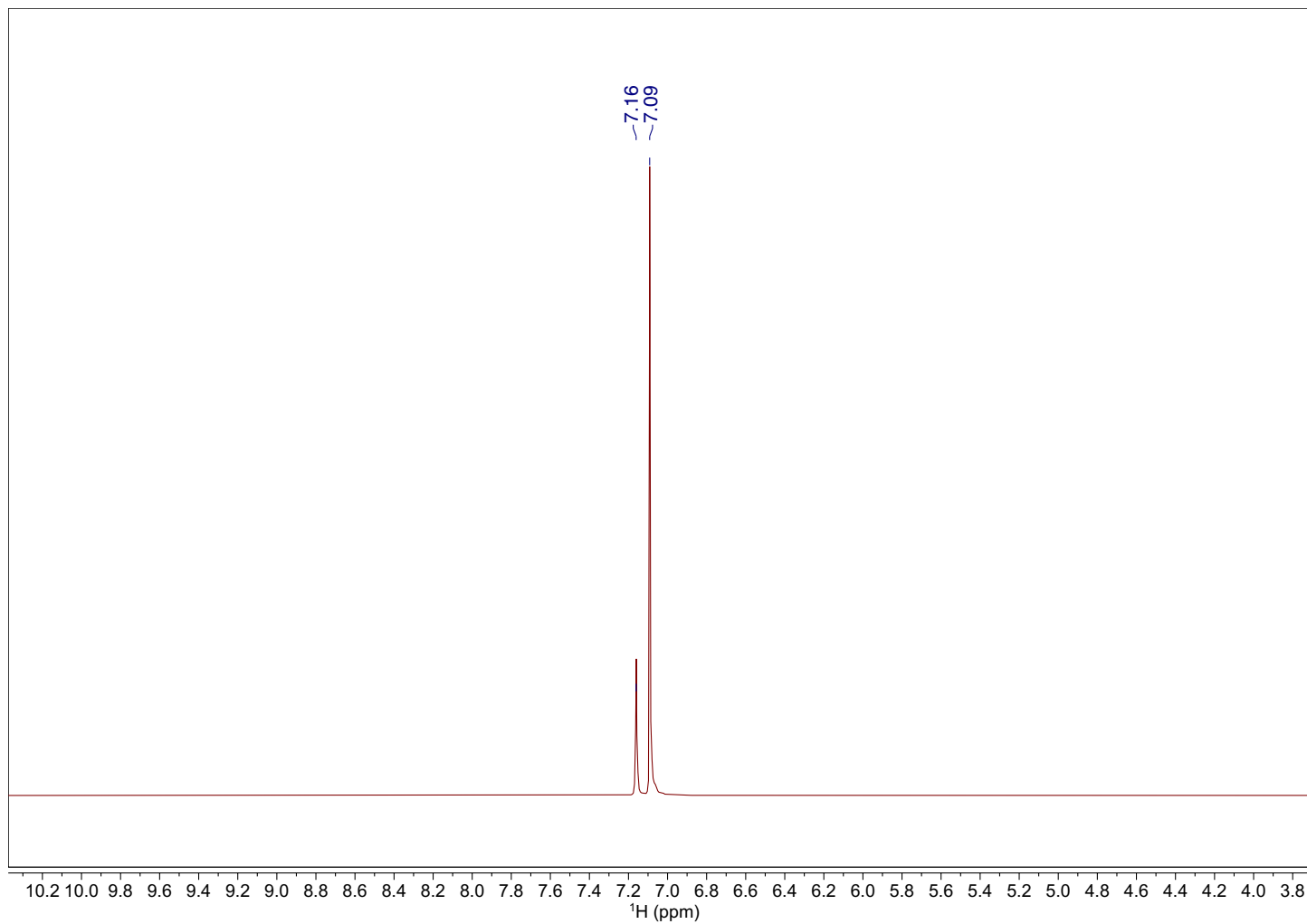


Figure S7. The ^1H NMR used for Evans' method magnetic moment determination of $\text{UK}(\mu\text{-SAr}^{\text{iPr}_6})_2$, **3**, in C_6D_6 . The concentration is 11 mM and an estimated diamagnetic correction of $-850 \times 10^{-6} \text{ emu mol}^{-1}$ was used.

UV-Visible Spectra

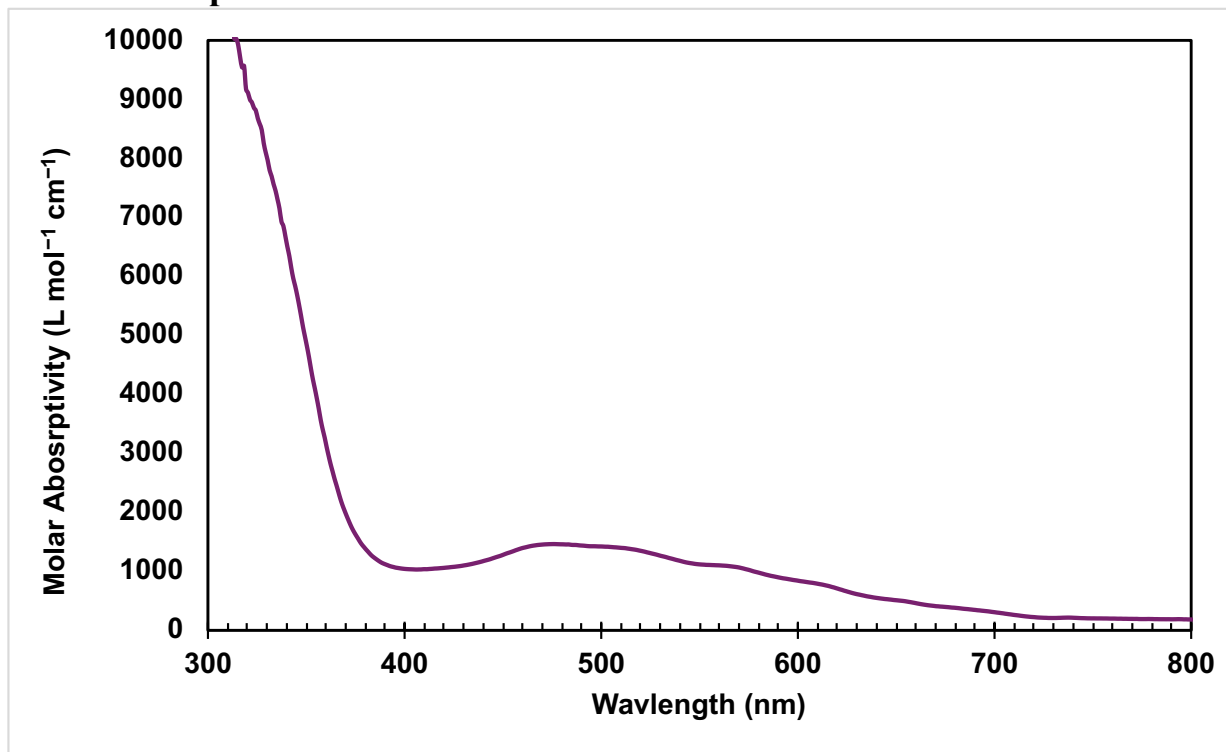


Figure S8. UV-visible absorbance spectrum of U(SAr^{iPr6})₂I, **1** in *n*-hexane.

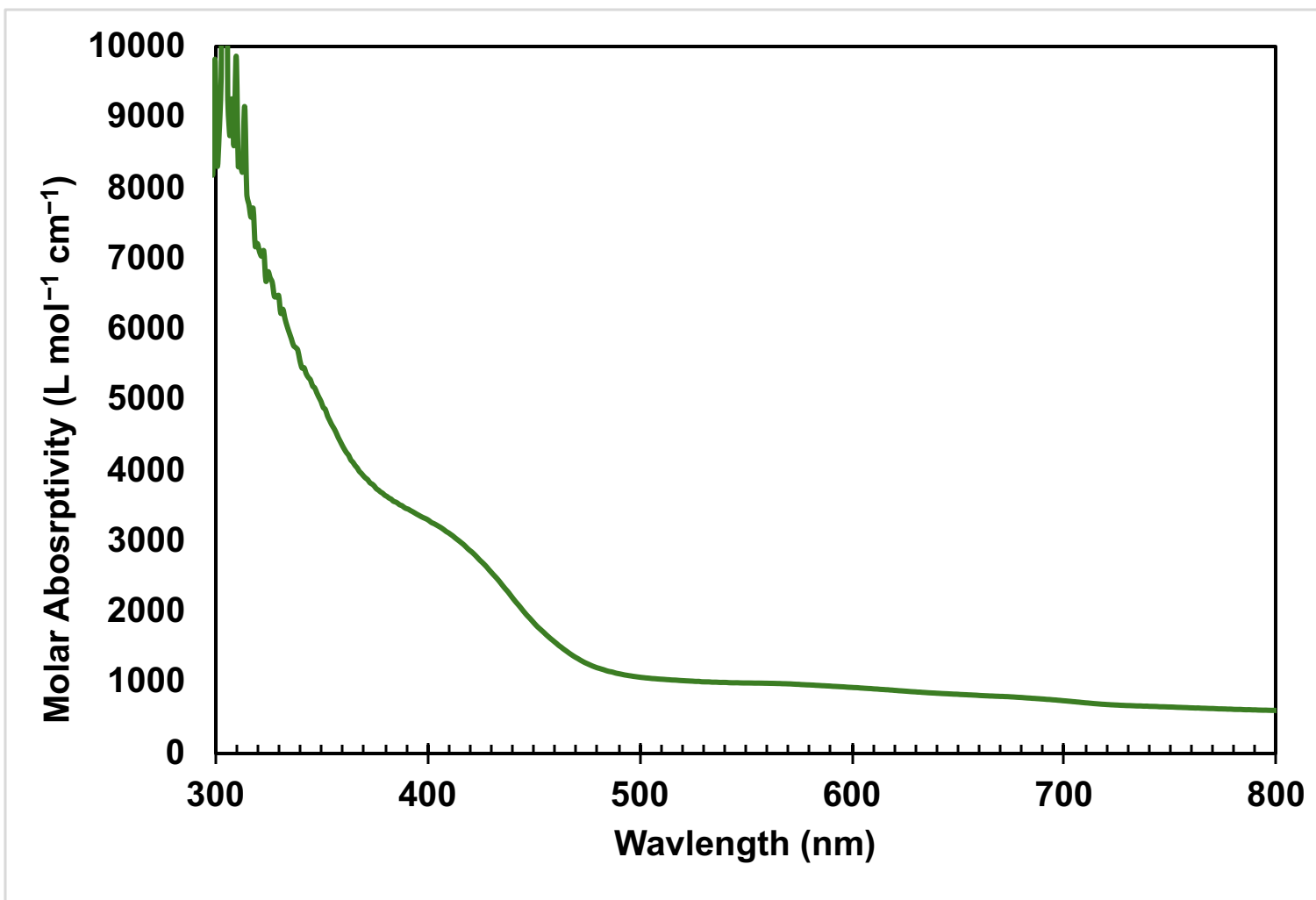


Figure S9. UV-visible absorbance spectrum of U(SAr^{iPr6})₂, **2**, in *n*-hexane.

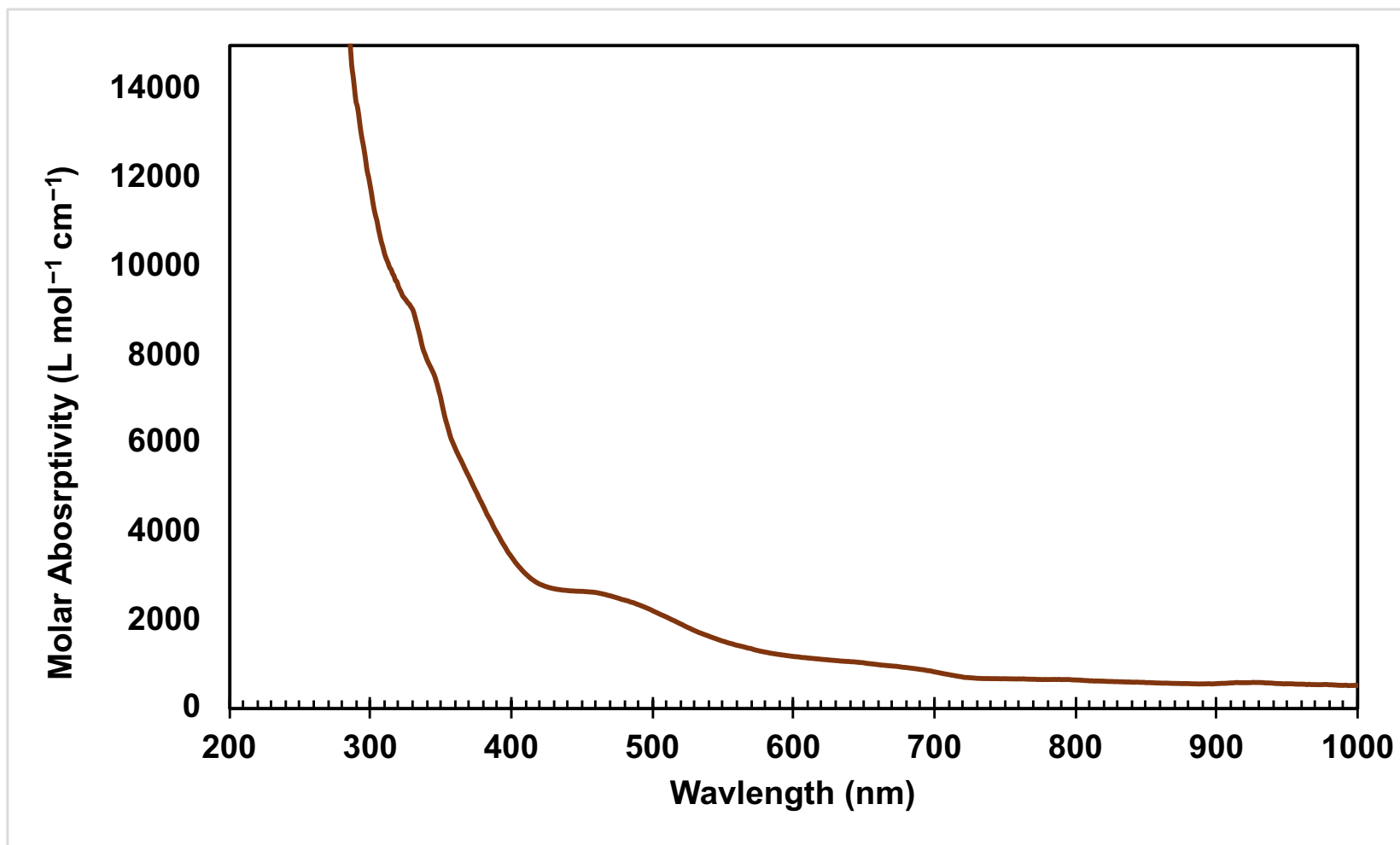


Figure S10. UV-visible absorbance spectrum of $U(SAr^{iPr6})_2(=NPh)_2(THF)_2$, **3** in *n*-hexane.

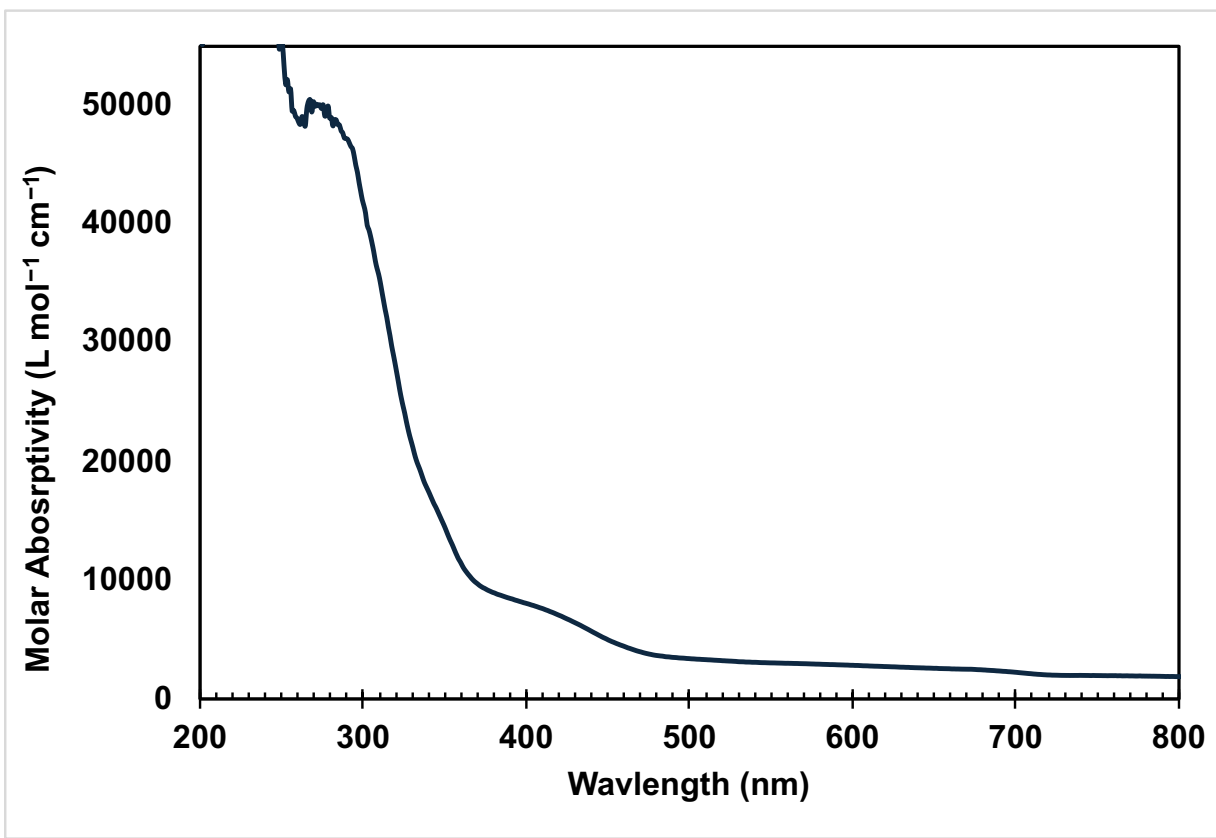


Figure S11. UV-visible absorbance spectrum of KU(SAr^{iPr6})₂, 4 in Et₂O.

Infrared Spectra

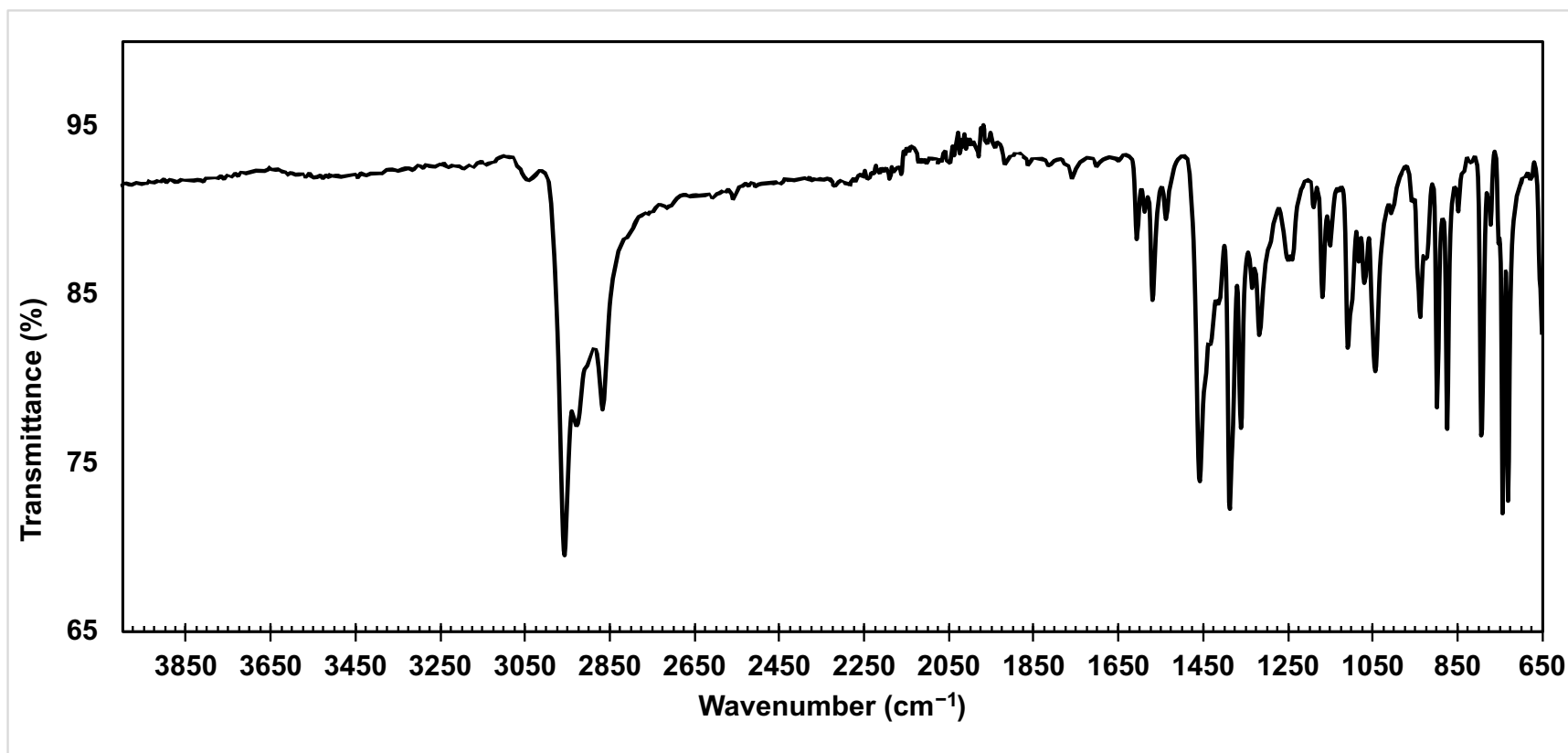


Figure S12. ATR-FTIR spectrum of U(SAr^{iPr6})₂I, **1**.

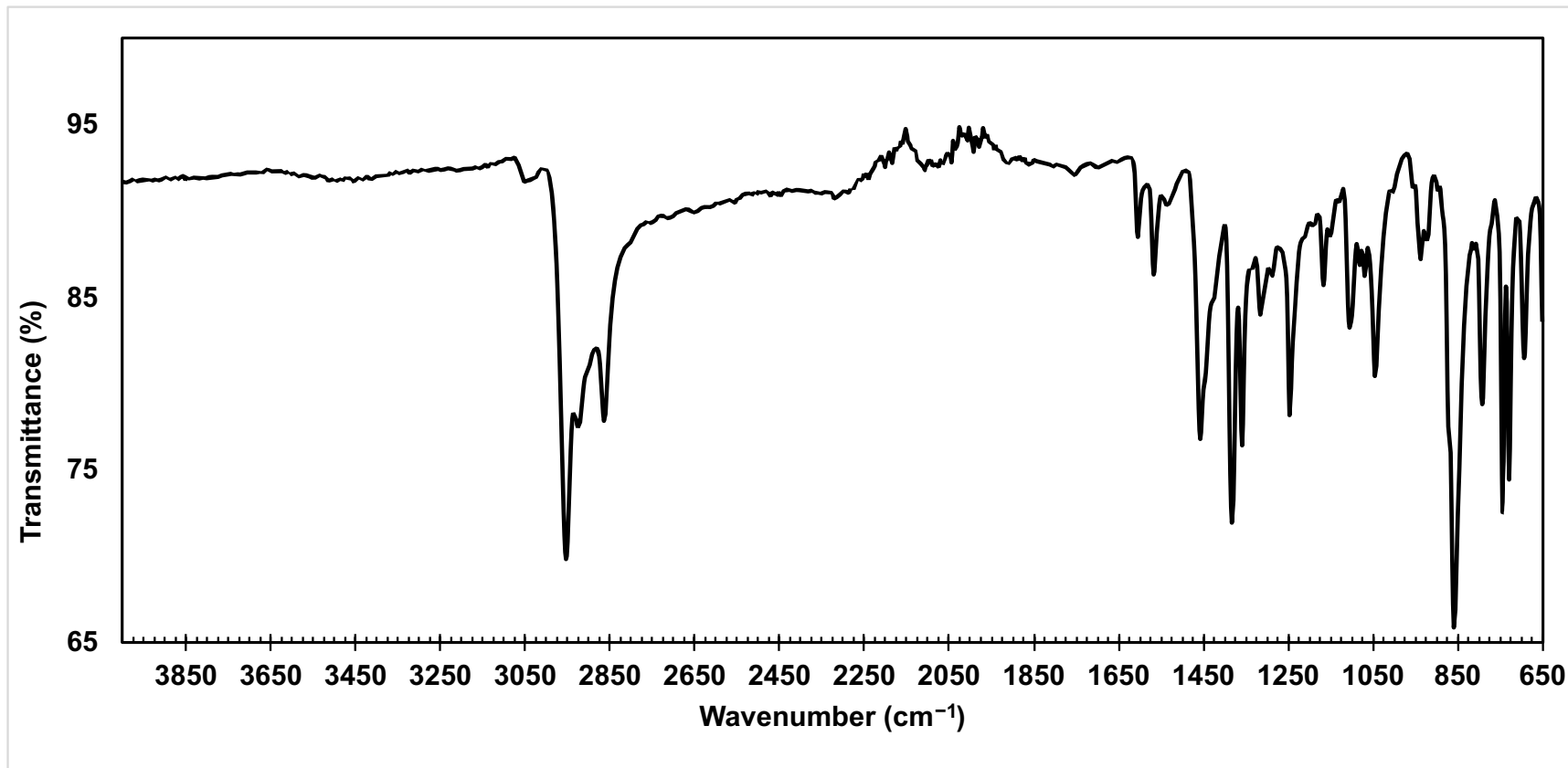


Figure S13. ATR-FTIR spectrum of $U(SAr^{iPr6})_2$, 2.

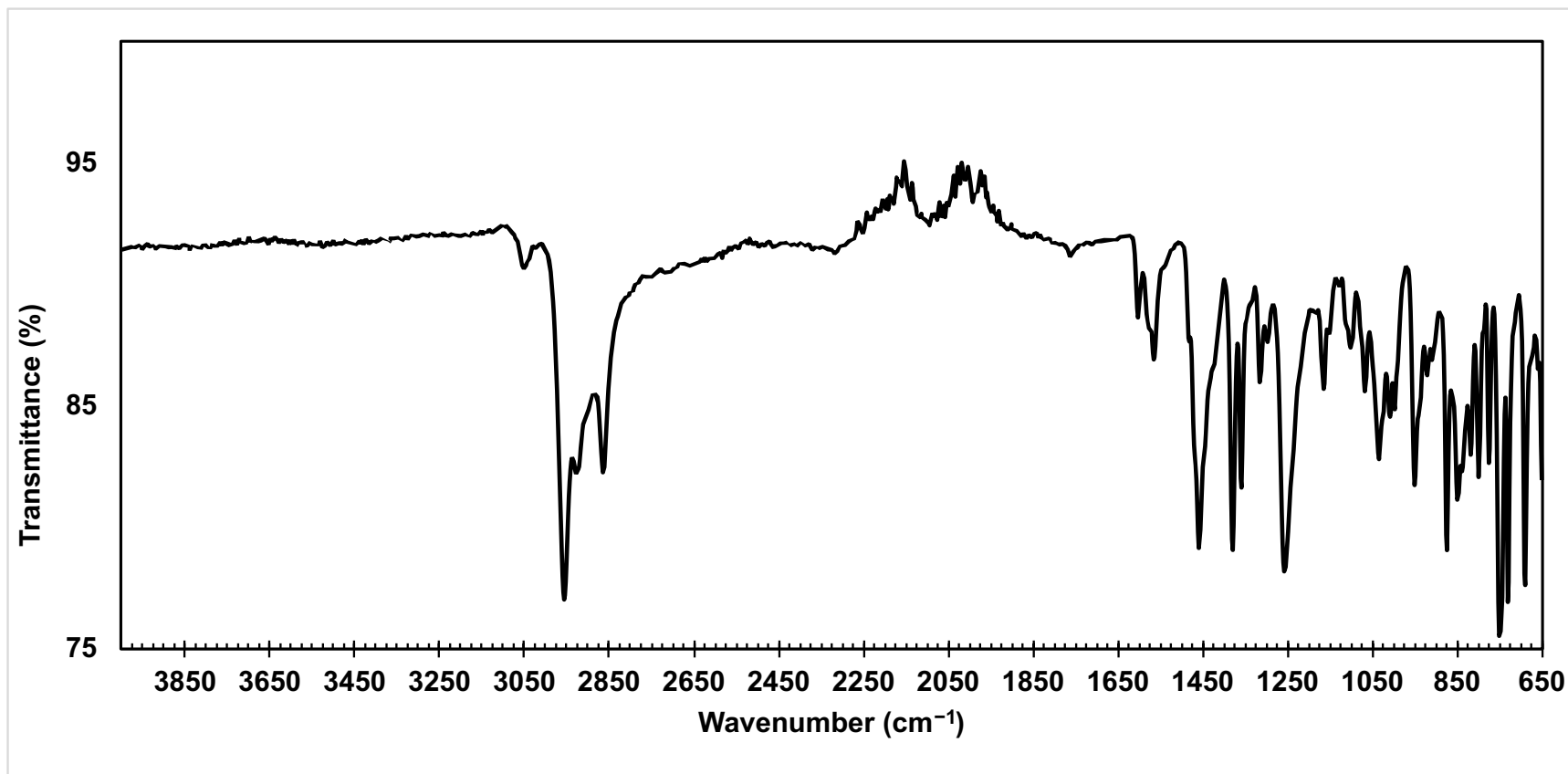


Figure S14. ATR-FTIR spectrum of $\text{U}(\text{SAr}^{\text{iPr}_6})_2(=\text{NPh})_2(\text{THF})_2$, **3**.

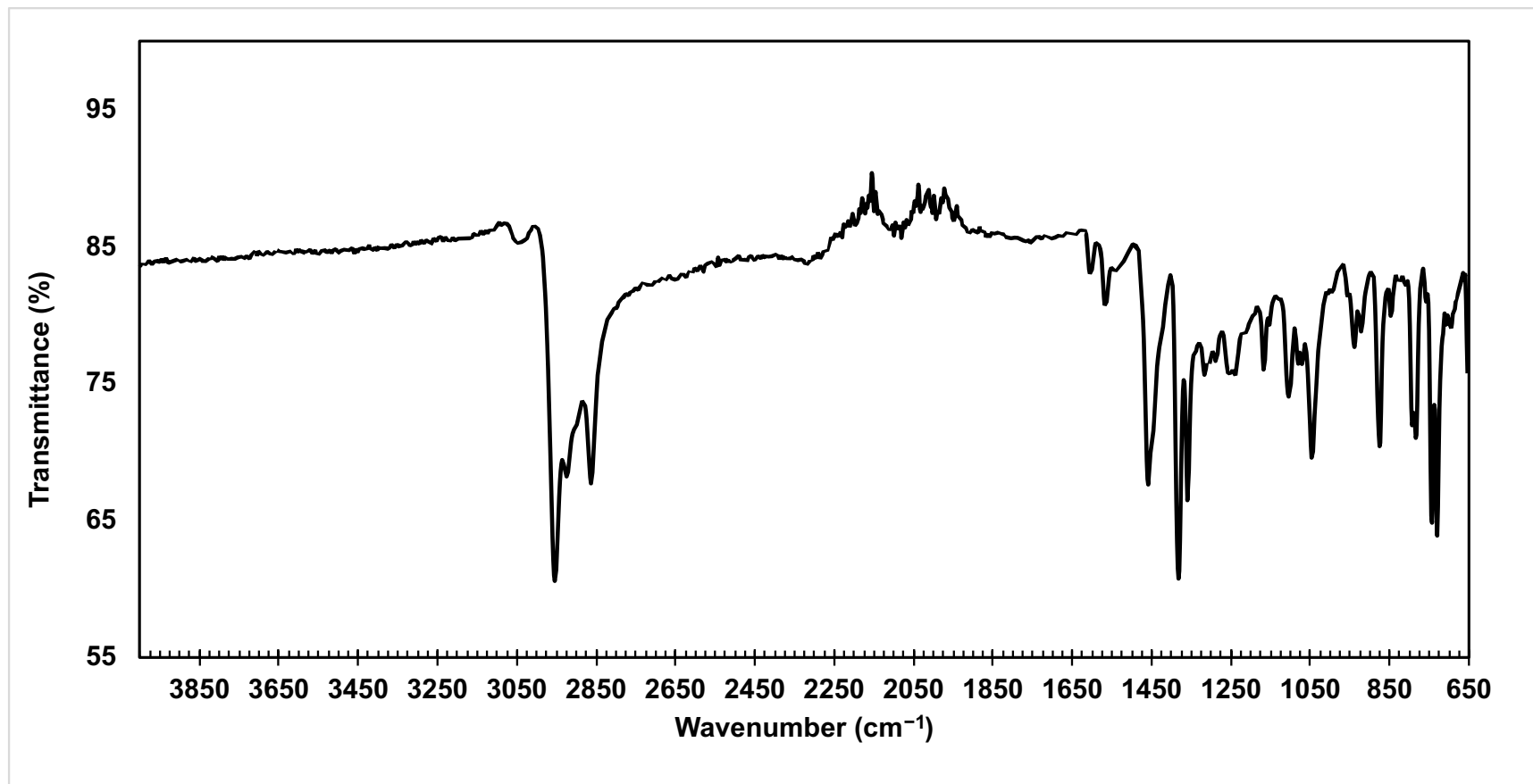


Figure S15. ATR-FTIR spectrum of $\text{KU}(\mu\text{-SAr}^{\text{iPr}_6})_2$, **4**.

Computational Details.

Density Functional Theory (DFT) was employed to study the electronic structure of the $\text{U}(\text{SAr}^{i\text{Pr}_6})_2$, **2**, and $\text{KU}(\mu\text{-SAr}^{i\text{Pr}_6})_2$, **4**, compounds. Geometry optimizations were performed on structures obtained from single-crystal X-ray diffraction. Split-valence basis sets with polarization functions on all non-hydrogen atoms, def2-SV(P)²¹, were used for C, H, S, K atoms, and triple-zeta quality basis sets, def-TZVP²², with scalar-relativistic effective core potentials (60 core electrons, def-ecp²³) were used for uranium. The TPSSh²⁴ functional with D3 dispersion corrections²⁵ and the Becke-Johnson damping function²⁶ were used to optimize the structures in both the gas and solution phases. DFT quadrature grids²⁷ were of size 4 with an energy convergence threshold of 10^{-7} a.u. and a one-electron density convergence threshold of 10^{-7} a.u. The maximum norm of the Cartesian energy gradient was set to 10^{-4} a.u. The resolution of identity (RI-J) approximation²⁸ was also used. Fermi smearing of Kohn-Sham occupation numbers was used to obtain desired spin states,^{29,30} as shown to be useful in systems with near-degenerate electronic configurations.³¹ The initial temperature was set to 3000 K, while the final temperature was set to 100 K using an annealing factor of 0.65. Occupation numbers were fixed during the smearing procedure to enforce the target spin state. Kohn-Sham (KS) orbitals corresponding to different spin states of each structure were analyzed using Mulliken population³² analysis and natural bond orbital population analysis (NPA)³³.

The optimized structures were reoptimized with hexane solvation effects using the COSMO model,³⁴ with a dielectric constant of 1.887 and a refractive index of 1.3727. Local minima on the potential energy surface were confirmed by numerical force constant calculations.³⁵ Time Dependent DFT (TDDFT)³⁶ using a non-orthonormal Krylov subspace solver³⁷ was used to calculate the excited state properties and UV-vis spectra. The first 180 to 250 electronically excited states of the compounds were computed in TDDFT calculations. The absorption spectrum of each compound was computed using a Gaussian lineshape with a half-width at half maximum (HWHM) of 0.2 eV centered on the excitation energies. This computational approach has proven effective for characterizing ground-state properties and simulating electronic spectra of large f-block organometallic complexes.^{31, 38-40}

The TURBOMOLE quantum chemistry package (version 7.8)⁴¹ was used for all the calculations. The VMD program⁴² was used to visualize the molecular orbitals.

Results

Theoretical calculations are presented in the following sections: Section I details the optimized structures and electronic configurations corresponding to different spin states for $\text{U}(\text{SAr}^{i\text{Pr}_6})_2$, **2**, and $\text{KU}(\mu\text{-SAr}^{i\text{Pr}_6})_2$, **4**; Section II describes the UV-Vis spectral simulations and electronic transitions; and Section III provides a discussion of the results.

Section I. Ground-State Geometries and Energetics

A. Optimized Geometries for Different Spin States and Relative Energies

The $\text{KU}(\mu\text{-SAr}^{i\text{Pr}_6})_2$, **4**, complex underwent geometry optimization for the doublet, quartet, and sextet electronic states while singlet, triplet, and quintet states were optimized for $\text{U}(\text{SAr}^{i\text{Pr}_6})_2$, **2**. The optimized structures were verified to be local minima. The two arene ligands bound to

uranium, denoted by carbons 14, 15, 16, 18, 19, 21 and carbons 99, 100, 101, 103, 104, 106 in the crystal structure, will be called arene 1 and arene 2, respectively. Geometry optimizations of $U(SAr^{iPr6})_2$, **2**, for the singlet and quintet states were also run for comparison. The arene ligands denoted by carbons 13, 14, 15, 17, 18, 20 and carbons 98, 99, 100, 103, 105 in the crystal structure (of **2**) will also be called arene 1 and 2 for comparison with **4**. A summary of the structural data for **2** is reported in **Tables S5, S6, S7** while the structural data for **4** is reported in **Tables S8, S9, S10**. The triplet and quintet states of **2** and the quartet and sextet states of **4** were found to be similar in energy, so a comparison of their energies calculated with different density functionals is tabulated in **Tables S11 and S12** respectively.

Table S5. Selected structural parameters (bond distances (Å) and angles (°)) from the crystal structure and computed electronic states for the $U(SAr^{iPr6})_2$, **2**, complex from DFT calculations using TPSSh, def-TZVP basis set for U, and def2-SV(P) basis sets for C, H, S. The relative energy is in reference to the lowest energy state. C–C(avg) is the average C–C bond distance of the arene rings.

	Singlet	Triplet	Quintet	X-Ray
U-Centroid(1) (Å)	2.28	2.27	2.38	2.348
U-Centroid(2) (Å)	2.28	2.63	2.46	2.522
Cnt(1)-U-Cnt(2) (°)	148.5	165.12	163.3	152.0
C–C(avg) (1) (Å)	1.42±0.03	1.43±0.03	1.42±0.02	1.42±0.02
C–C(avg) (2) (Å)	1.43±0.03	1.414±0.004	1.42±0.01	1.42±0.03
Relative energy (kcal/mol)	19.71	3.33	0	-

Table S6. Bond distances between each adjacent carbon in arenes 1 and 2 for $U(SAr^{iPr6})_2$, **2**. Atoms are numbered in increasing order in reference to their corresponding number in the crystal structure.

	Arene 1				Arene 2			
	Singlet	Triplet	Quintet	X-Ray	Singlet	Triplet	Quintet	X-Ray
C1-C2 (Å)	1.45	1.45	1.44	1.42	1.45	1.418	1.43	1.45
C2-C3 (Å)	1.44	1.44	1.42	1.42	1.44	1.409	1.41	1.46
C3-C4 (Å)	1.39	1.39	1.40	1.40	1.39	1.409	1.41	1.40
C4-C5 (Å)	1.44	1.45	1.43	1.45	1.44	1.412	1.43	1.40
C5-C6 (Å)	1.45	1.45	1.42	1.42	1.45	1.415	1.42	1.40
C6-C1 (Å)	1.40	1.40	1.41	1.41	1.40	1.420	1.41	1.39
Average (Å)	1.43	1.43	1.42	1.42	1.43	1.418	1.42	1.42
St. Dev.	0.03	0.03	0.02	0.02	0.03	0.004	0.01	0.03

Table S7. Dihedral angles in arenes 1 and 2 for $U(SAr^{iPr6})_2$, **2**. Atoms are numbered in increasing order in reference to their corresponding number in the crystal structure.

	Arene 1				Arene 2			
	Singlet	Triplet	Quintet	X-Ray	Singlet	Triplet	Quintet	X-Ray
C1-C2-C3-C4 (°)	-17.37	-16.60	-8.22	-14.41	-17.32	-1.13	-5.73	-8.18
C2-C3-C4-C5 (°)	-5.75	-3.66	-1.97	-2.11	-5.81	-5.29	-1.71	1.45

C3-C4-C5-C6 (°)	24.56	21.62	11.25	23.18	24.58	6.83	8.12	2.10
C4-C5-C6-C1 (°)	-19.91	-19.04	-10.02	-27.22	-19.89	-1.91	-6.85	1.71
C5-C6-C1-C2 (°)	-3.96	-1.72	-0.60	11.16	-4.00	-4.80	-0.93	-8.88
C6-C1-C2-C3 (°)	22.10	19.21	9.46	10.00	22.1	6.28	7.04	11.65

Table S8. Selected structural parameters (bond distances (Å) and angles (°)) from the crystal structure and computed electronic states for the $\text{KU}(\mu\text{-SAr}^{i\text{Pr}_6})_2$, **4**, complex from DFT calculations using TPSSh, def-TZVP basis set for U, and def2-SV(P) basis sets for C, H, S, K. The relative energy is in reference to the lowest energy state. C–C(avg) is the average C–C bond distance of benzene.

	Doublet	Quartet	Sextet	X-Ray
U-Centroid(1) (Å)	2.29	2.25	2.35	2.320
U-Centroid(2) (Å)	2.28	2.35	2.33	2.417
Cnt(1)-U-Cnt(2) (°)	131.3	129.4	133.0	130.08
C–C(avg) (1) (Å)	1.43±0.02	1.44±0.04	1.43±0.009	1.43±0.02
C–C(avg) (2) (Å)	1.43±0.03	1.42±0.008	1.43±0.02	1.41±0.01
Relative energy (kcal/mol)	6.67	0	5.43	-

Table S9. Bond distances between each adjacent carbon in arenes 1 and 2 for $\text{KU}(\mu\text{-SAr}^{i\text{Pr}_6})_2$, **4**. Atoms are numbered in increasing order in reference to their corresponding number in the crystal structure.

	Arene 1				Arene 2			
	Doublet	Quartet	Sextet	X-Ray	Doublet	Quartet	Sextet	X-Ray
C1-C2	1.44	1.47	1.43	1.44	1.47	1.42	1.45	1.42
C2-C3	1.45	1.45	1.43	1.44	1.40	1.43	1.41	1.40
C3-C4	1.39	1.38	1.41	1.41	1.42	1.41	1.41	1.39
C4-C5	1.44	1.45	1.42	1.42	1.46	1.42	1.43	1.41
C5-C6	1.44	1.46	1.43	1.45	1.40	1.43	1.41	1.42
C6-C1	1.41	1.40	1.43	1.40	1.42	1.43	1.43	1.40
Average	1.43	1.44	1.42	1.43	1.43	1.42	1.43	1.41
St. Dev.	0.02	0.04	0.009	0.02	0.03	0.008	0.02	0.01

Table S10. Dihedral angles in arenes 1 and 2 for $\text{KU}(\mu\text{-SAr}^{i\text{Pr}_6})_2$, **4**. Atoms are numbered in increasing order in reference to their corresponding number in the crystal structure.

	Arene 1				Arene 2			
	Doublet	Quartet	Sextet	X-Ray	Doublet	Quartet	Sextet	X-Ray
C1-C2-C3-C4 (°)	-12.87	-20.87	-2.22	-17.93	10.96	0.46	3.56	-2.91
C2-C3-C4-C5 (°)	-4.96	-2.79	-6.19	-4.81	-1.6	-8.02	-3.67	-7.03
C3-C4-C5-C6 (°)	19.78	25.55	9.91	25.11	-8.31	10.21	1.44	11.25
C4-C5-C6-C1 (°)	-16.63	-24.24	-5.31	-22.64	8.38	-4.98	0.75	-5.76
C5-C6-C1-C2 (°)	-1.79	-0.19	-3.42	-0.79	1.44	-2.9	-0.88	-4.38

C6-C1-C2-C3 (°)	16.11	22.05	7.04	20.53	-10.79	5.07	-1.22	8.58
-----------------	-------	-------	------	-------	--------	------	-------	------

Table S11. Spin state energy differences for $U(SAr^{iPr6})_2$, **2**, predicted by different functionals. Def2-SV(P) basis sets were used for all light atoms, and triple-zeta quality basis sets def-TZVP with small-core effective core potentials def-ecp were used for uranium.

Functional	Energy splitting ($E_{\text{triplet}} - E_{\text{quartet}}$) (kcal/mol)
TPSS	3.72
TPSSh	3.33
PBE0	2.72
B3LYP	1.51

Table S12. Spin state energy differences for $KU(\mu-SAr^{iPr6})_2$, **4**, predicted by different functionals. Def2-SV(P) basis sets were used for all light atoms, and triple-zeta quality basis sets def-TZVP with small-core effective core potentials def-ecp were used for uranium.

Functional	Energy splitting ($E_{\text{sextet}} - E_{\text{quartet}}$) (kcal/mol)
TPSS	4.56
TPSSh	5.43
PBE0	5.55
B3LYP	5.91

B. Population Analyses of Kohn-Sham Molecular Orbitals

NPA analysis was performed for both compounds for all spin states of both compounds. Molecular orbitals were visualized using Mulliken populations for both compounds for their respective lowest energy states. The atomic populations from total density and spin density are reported in **Table S13** and **Table S14**, respectively, for **2**, and in **Table S17** and **S18**, respectively, for **4**. The five highest occupied molecular orbitals (HOMO) and the lowest unoccupied molecular orbital (LUMO) were tabulated and reported in **Table S15** for **2** and **Table S189** for **4**. The atomic populations of the U atom and the two arenes for the reported occupied orbitals are tabulated in **Table S16** for **2** and **Table S20** for **4**.

Table S13. Atomic populations of the U atom for singlet, triplet, quintet spin states of $U(SAr^{iPr6})_2$, **2**, from total density from NPA.

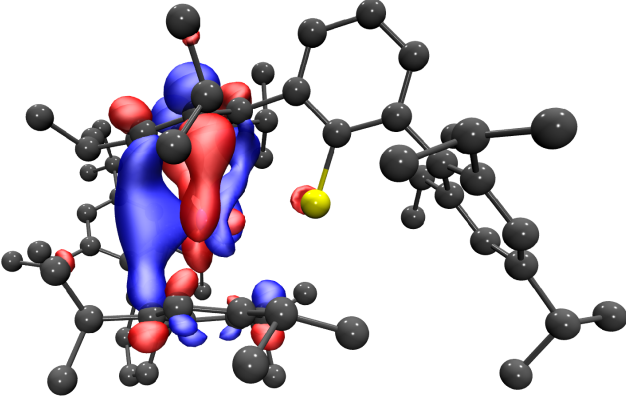
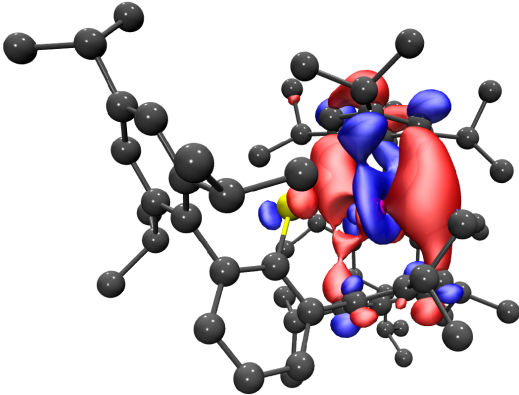
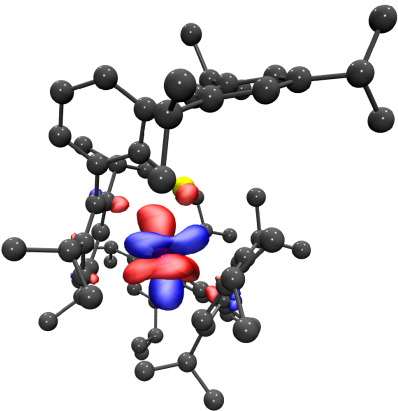
	Charge	n(s)	n(p)	n(d)	n(f)
Singlet	0.23	4.21	11.99	11.87	3.70
Triplet	0.60	4.20	11.99	11.62	3.59
Quintet	0.51	4.21	12.00	11.71	3.58

Table S14. Atomic populations of the quintet state of $U(SAr^{iPr6})_2$, **2**, complex from spin density from NPA. Arenes 1 and 2 imply the sum over all carbons of each benzene bound to U.

		Sum	n(s)	n(p)	n(d)	n(f)
Triplet	U	2.80	0.02	0.02	0.22	2.55
	Arene 1	-0.13	0.00	-0.12	-	-
	Arene 2	0.31	0.01	0.30	-	-

Quintet	U	3.29	0.04	0.02	0.39	2.83
	Arene 1	0.36	0.01	0.35	-	-
	Arene 2	0.19	0.01	0.19	-	-

Table S15. Visualized molecular orbitals and corresponding energies for the quintet state of $U(\text{SAr}^{i\text{Pr}_6})_2$, **2**. Hydrogen atoms are omitted for clarity, and a contour value of 0.04 was used in the orbital visualizations.

Molecular Orbital		Energy (eV)
LUMO (α)		-2.018
HOMO (α)		-3.219
HOMO-1 (α)		-3.858

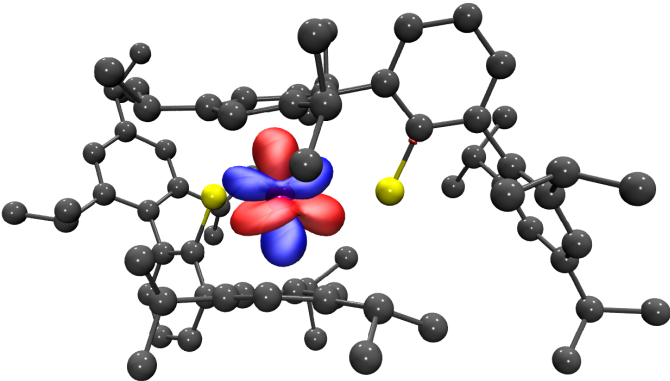
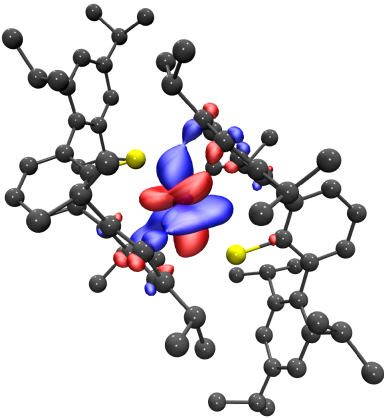
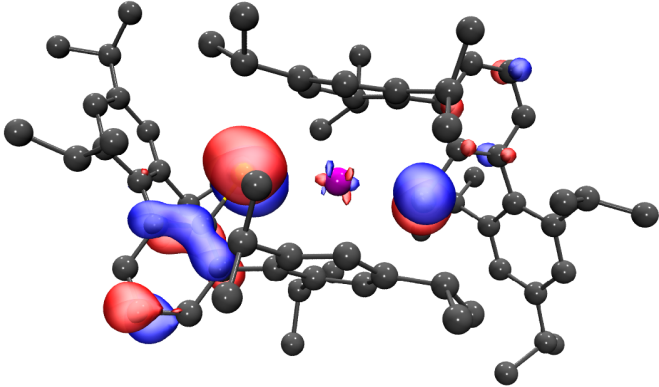
HOMO-2 (α)		-3.893
HOMO-3 (α)		-3.940
HOMO-4 (α)		-5.023

Table S16. Atomic populations for d and f orbitals of uranium and all orbitals for arene 1 and 2 from total density for the 5 highest occupied orbitals of the quintet state of $U(\text{SAr}^{\text{iPr}_6})_2$, **2**, from NPA. Arenes 1 and 2 imply the combined total of the sum over all orbital populations for each carbon in each benzene bound to U.

	HOMO	HOMO-1	HOMO-2	HOMO-3	HOMO-4
d orbitals	0.24	0.006	0.01	0.01	0.006
f orbitals	0.14	0.84	0.93	0.83	0.07
Arene 1	0.26	0.04	0.006	0.06	0.006
Arene 2	0.11	0.04	0.009	0.05	0.007

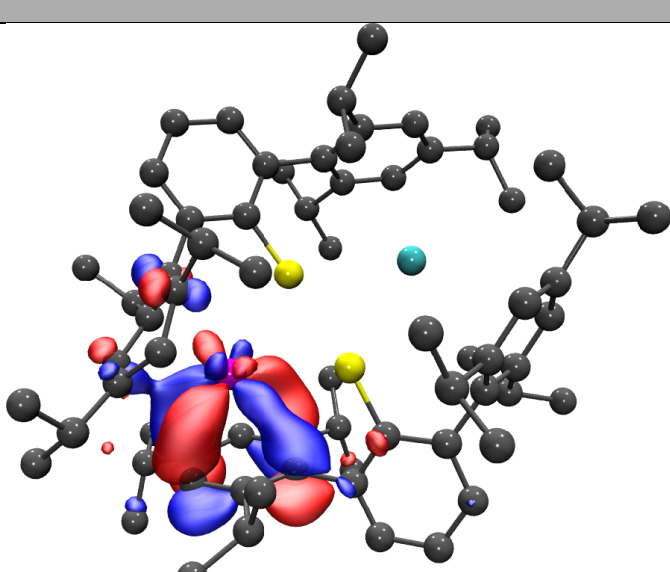
Table S17. Atomic populations of the U atom for doublet, quartet, sextet spin states of $\text{KU}(\mu\text{-SAr}^{i\text{Pr}_6})_2$, **4**, from total density from NPA.

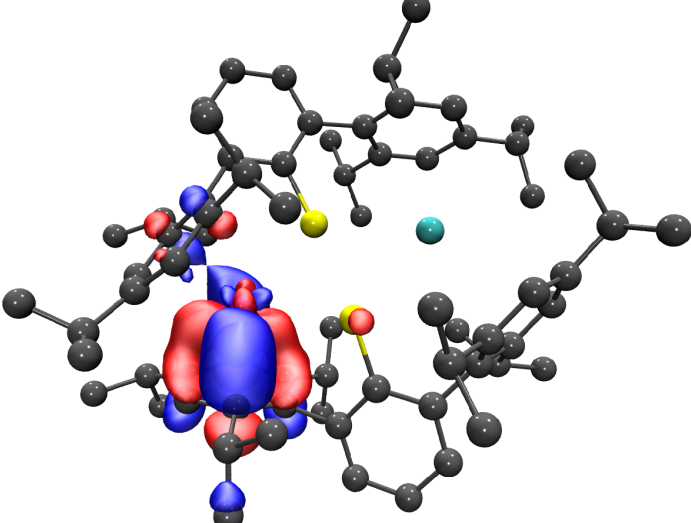
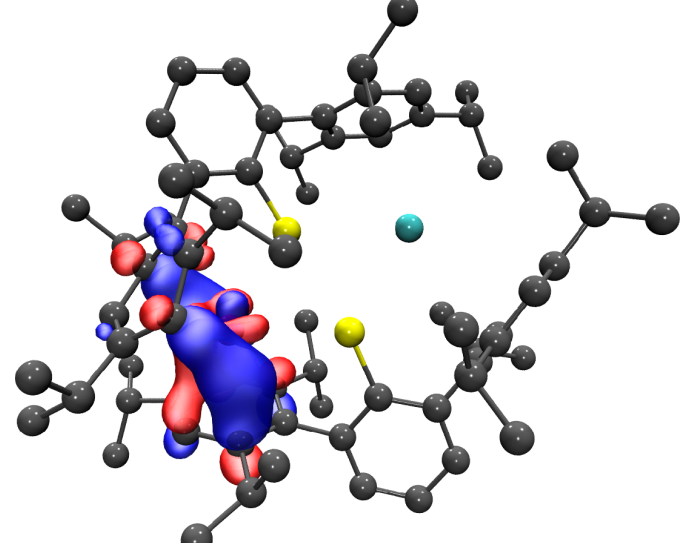
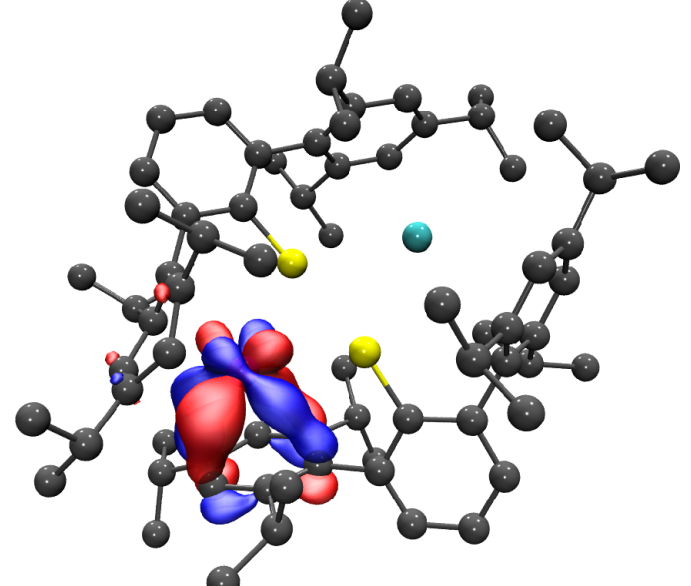
	Charge	n(s)	n(p)	n(d)	n(f)
Doublet	0.40	4.21	11.99	11.75	3.65
Quartet	0.41	4.23	11.99	11.81	3.55
Sextet	0.37	4.20	12.00	11.71	3.72

Table S18. Atomic populations from spin density for the doublet, quartet, sextet states of the $\text{KU}(\mu\text{-SAr}^{i\text{Pr}_6})_2$, **4**, complex from NPA. Arenes 1 and 2 imply the sum over all carbons of each benzene bound to U.

		Sum	n(s)	n(p)	n(d)	n(f)
Doublet	U	1.83	-0.02	0.02	-0.25	2.08
	Arene 1	-0.40	-0.02	-0.38	-	-
	Arene 2	-0.31	-0.01	-0.31	-	-
Quartet	U	2.80	0.02	0.02	0.22	2.55
	Arene 1	-0.13	0.00	-0.12	-	-
	Arene 2	0.31	0.01	0.30	-	-
Sextet	U	3.74	0.05	0.04	0.63	3.02
	Arene 1	0.49	0.02	0.47	-	-
	Arene 2	0.58	0.01	0.57	-	-

Table S19. Visualized molecular orbitals and corresponding energies for the quartet state of $\text{KU}(\mu\text{-SAr}^{i\text{Pr}_6})_2$, **4**. A contour value of 0.03 was used in the orbital visualization.

Molecular Orbital		Energy (eV)
LUMO (β)		-1.274

HOMO (β)		-2.774
HOMO-1 (α)		-2.810
HOMO-2 (α)		-3.026

HOMO-3 (α)		-3.190
HOMO-4 (α)		-3.348

Table S20. Atomic populations for d and f orbitals of uranium and all orbitals for arene **1** and **2** from total density for the 5 highest occupied orbitals of the quartet state of $\text{KU}(\mu\text{-SAr}^{i\text{Pr}_6})_2$, **4**, from NPA. Arenes 1 and 2 imply the combined total of the sum over all orbital populations for each carbon in each benzene bound to U.

	HOMO	HOMO-1	HOMO-2	HOMO-3	HOMO-4
d orbitals	0.21	0.25	0.06	0.004	0.03
f orbitals	0.15	0.29	0.71	0.84	0.74
Arene 1	0.43	0.14	0.04	0.04	0.15
Arene 2	0.07	0.18	0.14	0.07	0.01

Section II. Simulation and Characterization of Electronic Spectra from TDDFT

The first 200 and 250 electronic excitations were calculated for each spin state of **2** and **4**, respectively, and used to simulate UV-Vis spectra. The simulated spectra were plotted against experimental data and shown in **Fig S16** for **2** and **Fig S17** for **4**. The major excitations for the lowest energy states are reported in **Table S20** for **2** and **Table S21** for **4**.

Table S21. Electronic excitation summary for quintet of U(SAr^{iPr6})₂, **2**, computed with TDDFT using TPSSh functional, def-TZVP basis set for U, and def-SV(P) basis sets for C, H, S, including COSMO solvent model. All excitations computed are single excitations involving alpha spin to alpha spin transitions. Oscillator strengths are reported in the length gauge. Only the dominant contributions to the overall excitation are reported.

Wavelength (nm)	Osc. (len.)	Occupied (eV)	Dominant Contributions		
			Unoccupied (eV)	% Weight	Exc. Type
456	0.0403	295 β (-5.10)	296 β (-1.96)	90.1	L \rightarrow δ
611	0.0361	299 α (-3.22)	304 α (-0.73)	33.5	$\delta \rightarrow \delta^*$
		298 α (-3.86)	304 α (-0.83)	15.6	M (f) $\rightarrow \delta^*$
		299 α (-3.22)	307 α (-0.59)	10.0	$\delta \rightarrow M-L^*$ (f- π^*)
296	0.0272	294 β (-5.14)	300 β (-0.68)	21.0	L \rightarrow L
		295 α (-5.02)	305 α (-0.68)	12.9	L \rightarrow M (f) / L
		295 β (-5.10)	300 β (-0.68)	11.2	L \rightarrow L
370	0.0250	295 β (-5.10)	300 β (-0.68)	39.3	L \rightarrow L
		295 α (-5.02)	305 α (-0.68)	13.4	L \rightarrow M (f) / L

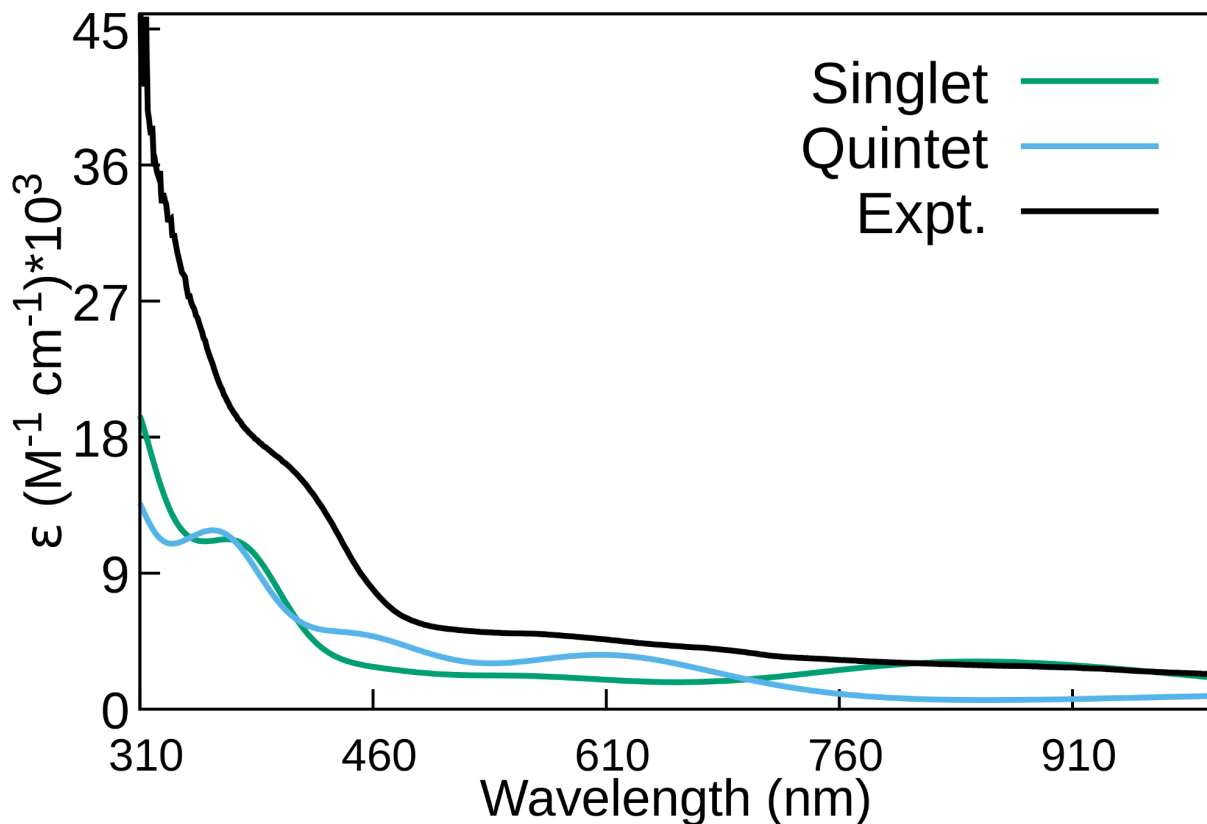


Figure S16. Simulated UV-vis of $U(SAr^{iPr6})_2$, **2**, from TDDFT calculations using TPSSh functional, def-TZVP basis set for U, and def2-SV(P) basis sets for C, H, S. The COSMO solvent model with hexane parameters was included. A Gaussian spectral lineshape with a HWHM of 0.2 eV was used.

Table S22. Electronic excitation summary for the quartet state of $KU(\mu-SAr^{iPr6})_2$, **4**, computed with TDDFT using TPSSh functional, def-TZVP basis set for U, and def2-SV(P) basis sets for C, H, S, including COSMO solvent model. All excitations computed are single excitations involving alpha spin to alpha spin transitions. Oscillator strengths are reported in the length gauge. Only the dominant contributions to the overall excitation are reported.

Wavelength (nm)	Osc. (len.)	Occupied (eV)	Dominant Contributions		
			Unoccupied (eV)	% Weight	Exc. Type
281	0.0367	304 α (-4.83)	322 α (-0.05)	27.8	L \rightarrow M (f) / L
		308 α (-2.84)	336 α (1.87)	9.1	$\delta \rightarrow$ L
335	0.0323	304 α (-4.83)	311 α (-0.85)	18.5	L \rightarrow L
		304 β (-4.80)	309 β (-0.83)	18.1	L \rightarrow L
		303 α (-5.04)	310 α (-0.96)	16.2	L \rightarrow δ
443	0.0295	307 α (-3.05)	324 α (0.57)	44.2	$\delta \rightarrow \delta^*$
		305 α (-3.37)	319 α (-0.24)	17.3	$\delta \rightarrow$ M (f) / L

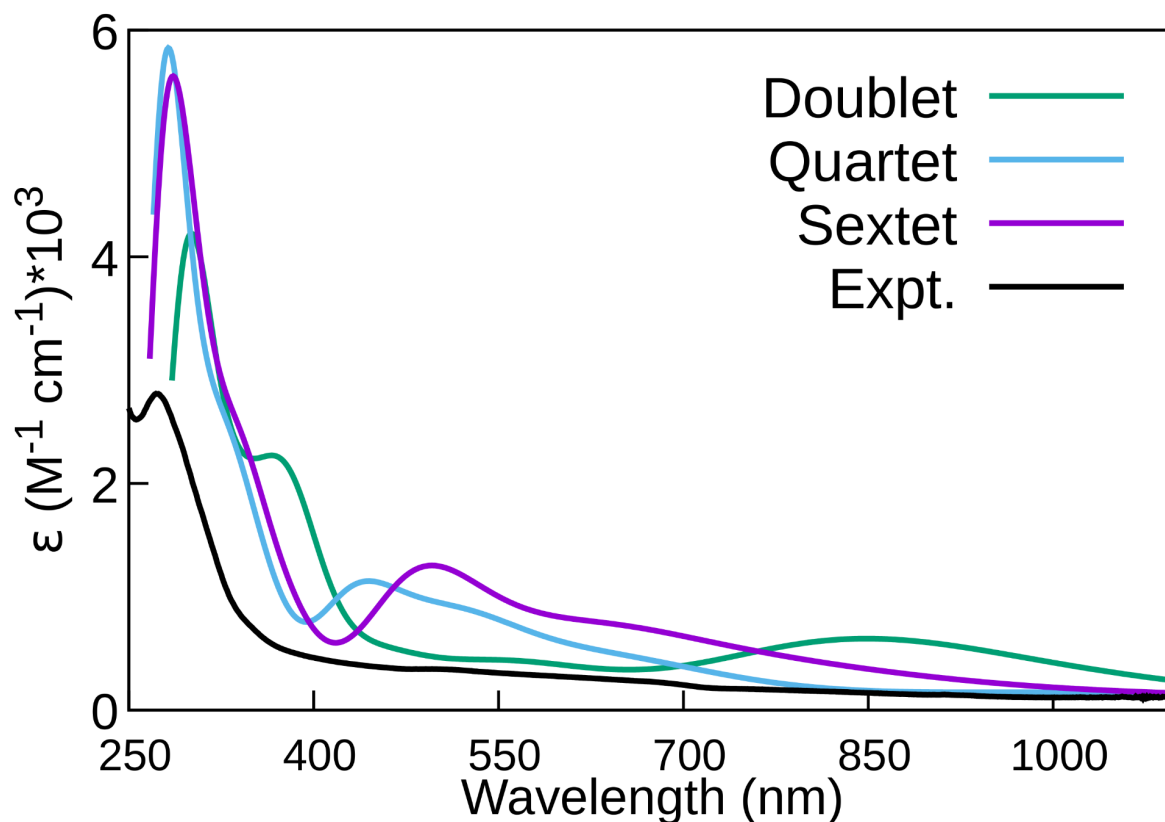


Figure S17. Simulated UV-vis of $\text{KU}(\mu\text{-SAr}^{i\text{Pr}_6})_2$, **4**, from TDDFT calculations using TPSSh functional, def-TZVP basis set for U, and def2-SV(P) basis sets for C, H, K, S. The COSMO solvent model with hexane parameters was included. A Gaussian spectral lineshape with a HWHM of 0.2 eV was used. The simulated spectra were scaled by a factor of 0.20.

Section III. Discussion

From the structural data, the quintet state of **2** is a closer match to experiment than the singlet or triplet. Namely, the centroid distances in **Table S5** of the quintet state are closer to the crystal structure than the other two spin states. While the triplet state is close in energy to the quintet, the triplet is consistently higher in energy for all density functionals tested as shown in **Table S11**. For **4**, the doublet state shows poor agreement with experiment overall. **Table S8** indicates that the quartet state preserves the relative centroid distances and is more energetically stable, although the sextet state is closer in absolute distance. The distortion of the two arene ligands of the crystal structure is best matched by the computed values of the quartet state, as quantified in **Table S10**. Thus, structural data seems to indicate a quintet ground state for **2** and quartet ground state for **4**. These assertions are supported by qualitative agreement of the quintet and quartet states to experimental data in the UV-vis spectra shown in **Fig S16** and **Fig S17**, respectively.

From **Table S15**, the HOMO of the quintet state of **2** shows mostly d orbital character with some f orbital admixing of the U atom δ -bonding to π^* orbitals of arene 1. HOMO-1 to HOMO-3 are nonbonding, consisting of f orbitals of the U atom. HOMO-4 was only visualized for consistency with **4** and is not relevant to discussion. The atomic populations for each orbital reported in **Table**

S16 support these qualitative assertions. These results suggest a $5f^36d^1$ ground state with minor $5f^4$ admixing. Combined with results from geometry optimization, these findings are consistent with early DFT studies that predicted neutral bis(arene)benzene complexes to exhibit bent structures and δ -bonding interactions.^{43,44}

According to **Table S19**, the HOMO of the quartet state of **4** shows mostly d orbital character with some f orbital admixing of the U atom δ -bonding to π^* orbitals of arene 2. The two orbitals below the HOMO show similar δ -bonding with greater contribution from arene 1. HOMO-2 to HOMO-4 have significant f orbital character. HOMO-3 shows δ -bonding of the U atom with arene 2 and some σ -bonding with arene 1. HOMO-4 shows mostly δ -bonding with arene 1. The atomic populations for each orbital reported in **Table S16** support these qualitative assertions. These results indicate the ground state is between $5f^36d^2$ and $5f^5$.

The significant delocalization over both the uranium and two arene ligands in the HOMO of both compounds means it is difficult to assign the electron to entirely the metal or ligand. The arenes of both compounds are significantly elongated and distorted across all structures, as shown **Table S6** and **Table S7** for **2** and **Table S9** and **Table S10** for **4**, implying significant charge delocalization over the rings.^{31,45} Similar metal-ligand bonding has been observed previously⁴³⁻⁴⁵ and has been described as polar covalent bonding between the d orbitals of the metal and the π^* orbitals of the arene.

References

1. G. R. Fulmer, A. J. M. Miller, N. H. Sherden, H. E. Gottlieb, A. Nudelman, B. M. Stoltz, J. E. Bercaw and K. I. Goldberg, *Organometallics*, 2010, **29**, 2176-2179.
2. D. F. Evans, *J. Chem. Soc.*, 1959, DOI: 10.1039/JR9590002003, 2003-2005.
3. S. K. Sur, *J. Magn. Reson.*, 1989, **82**, 169-173.
4. G. A. Bain and J. F. Berry, *J. Chem. Educ.*, 2008, **85**, 532.
5. M. Niemeyer and P. P. Power, *Inorg. Chem.*, 1996, **35**, 7264-7272.
6. C. D. Carmichael, N. A. Jones and P. L. Arnold, *Inorg. Chem.*, 2008, **47**, 8577-8579.
7. D. E. Bergbreiter and J. M. Killough, *J. Am. Chem. Soc.*, 1978, **100**, 2126-2134.
8. M. Roger, N. Barros, T. Arliguie, P. Thuéry, L. Maron and M. Ephritikhine, *J. Am. Chem. Soc.*, 2006, **128**, 8790-8802.
9. D. Pividori, M. E. Miehlich, B. Kestel, F. W. Heinemann, A. Scheurer, M. Patzschke and K. Meyer, *Inorg. Chem.*, 2021, **60**, 16455-16465.
10. B. L. L. Réant, J. A. Seed, G. F. S. Whitehead and C. A. P. Goodwin, *Inorg. Chem.*, 2025, **64**, 3161-3177.
11. D. R. Kindra and W. J. Evans, *Chem. Rev.*, 2014, **114**, 8865-8882.
- 12.(a) APEX2 Version 2014.11-0, Bruker AXS, Inc.; Madison, WI 2014. (b) APEX5 Version 2023.9-2, Bruker AXS, Inc.; Madison, WI 2023.
- 13.(a) SAINT Version 8.34a, Bruker AXS, Inc.; Madison, WI 2013. (b) SAINT Version 8.40b, Bruker AXS, Inc.; Madison, WI 2013

- 14.(a) G. M. Sheldrick, SADABS, Version 2014/5, Bruker AXS, Inc.; Madison, WI 2014. (b) G. M. Sheldrick, SADABS, Version 2016/2, Bruker AXS, Inc.; Madison, WI 2016
15. G. M. Sheldrick, SHELXTL, Version 2014/7, Bruker AXS, Inc.; Madison, WI 2014.
16. International Tables for Crystallography 1992, Vol. C., Dordrecht: Kluwer Academic Publishers.
17. G. M. Sheldrick, CELL_NOW, Version 2008/4, Bruker AXS, Inc.; Madison, WI 2008.
18. G. M. Sheldrick, TWINABS, Version 2012/1, Bruker AXS, Inc.; Madison, WI 2012.
19. A. L. Spek, *Acta. Cryst.*, 2015, C71, 9-19.
20. A. L. Spek, *Acta. Cryst.*, 2009, D65, 148-155.
21. A. Schäfer, H. Horn and R. Ahlrichs, *J. Chem. Phys.*, 1992, **97**, 2571–2577.
22. F. Weigend and R. Ahlrichs, *Phys. Chem. Chem. Phys.*, 2005, **7**, 3297–3305.
23. M. Dolg, H. Stoll and H. Preuss, *J. Chem. Phys.*, 1989, **90**, 1730–1734.
24. V. N. Staroverov, G. E. Scuseria, J. Tao and J. P. Perdew, *J. Chem. Phys.*, 2003, **119**, 12129–12137.
25. S. Grimme, J. Antony, S. Ehrlich and H. Krieg, *J. Chem. Phys.*, 2010, **132**, 154104.
26. S. Grimme, S. Ehrlich and L. Goerigk, *J. Comput. Chem.*, 2011, **32**, 1456–1465.
27. O. Treutler and R. Ahlrichs, *J. Chem. Phys.*, 1995, **102**, 346–354.
28. K. Eichkorn, O. Treutler, H. Öhm, M. Häser and R. Ahlrichs, *Chem. Phys. Lett.*, 1995, **240**, 283–290.
29. A. D. Rabuck and G. E. Scuseria, *J. Chem. Phys.*, 1999, **110**, 695–700.
30. P. Nava, M. Sierka and R. Ahlrichs, *Phys. Chem. Chem. Phys.*, 2003, **5**, 3372–3381.
31. K. R. McClain, A. H. Vincent, A. Rajabi, D. X. Ngo, K. R. Meihaus, F. Furche, B. G. Harvey and J. R. Long, *J. Am. Chem. Soc.*, 2024, **146**, 32708–32716.
32. R. S. Mulliken, *J. Chem. Phys.*, 1955, **23**, 1833–1840.
33. A. E. Reed, R. B. Weinstock and F. Weinhold, *J. Chem. Phys.*, 1985, **83**, 735–746.
34. A. Klamt and G. Schüürmann, *J. Chem. Soc., Perkin Trans. 2*, 1993, 799–805.
35. P. Deglmann, K. May, F. Furche and R. Ahlrichs, *Chem. Phys. Lett.*, 2004, **384**, 103–107.
36. R. Bauernschmitt and R. Ahlrichs, *Chem. Phys. Lett.*, 1996, **256**, 454–464.
37. F. Furche, B. T. Krull, B. D. Nguyen and J. Kwon, *J. Chem. Phys.*, 2016, **144**, 174105.
38. A. Rajabi, R. Grotjahn, D. Rappoport and F. Furche, *Dalton Trans.*, 2024, **53**, 410–417.
39. M. R. MacDonald, M. E. Fieser, J. E. Bates, J. W. Ziller, F. Furche and W. J. Evans, *J. Am. Chem. Soc.*, 2013, **135**, 13310–13313.
40. MacDonald, M. R.; Fieser, M. E.; Bates, J. E.; Ziller, J. W.; Furche, F.; Evans, W. J. Identification of the + 2 Oxidation State for Uranium in a Crystalline Molecular Complex, [K(2.2.2-Cryptand)][(C₅H₄SiMe₃)₃U]. *J. Am. Chem. Soc.* 2013, **135**, 13310– 13313.
41. Y. J. Franzke, C. Holzer, J. H. Andersen, T. Begušić, F. Bruder, S. Coriani, F. Della Sala, E. Fabiano, D. A. Fedotov, S. Furst, S. Gillhuber, R. Grotjahn, M. Kaupp, M. Kehry, M. Krstić, F. Mack, S. Majumdar, B. D. Nguyen, S. M. Parker, F. Pauly, A. Pausch, E. Perlt, G. S. Phun, A. Rajabi, D. Rappoport, B. Samal, T. Schrader, M. Sharma, E. Tapavicza, R. S. Treß, V.

- Voorra, A. Wodyński, J. M. Yu, B. Zerulla, F. Furche, C. Hättig, M. Sierka, D. P. Tew and F. Weigend, *J. Chem. Theory Comput.*, 2023, **19**, 6859–6890.
42. W. Humphrey, A. Dalke and K. Schulten, *J. Mol. Graphics.*, 1996, **14**, 33–38.
43. Li and B. E. Bursten, *J. Am. Chem. Soc.*, 1999, **121**, 10243–10244.
44. N. Kaltsoyannis, *Chem. Soc. Rev.*, 2003, **32**, 9–16.
45. S. R. Chowdhury, C. A. P. Goodwin and B. Vlasisavljevich, *Chem. Sci.*, 2024, **15**, 1810–1819.